

Bathing in a sea of candidate quantum spin liquids: From the gapless ruby to the gapped maple-leaf lattice

Philipp Schmoll,^{1,*} Jan Naumann,^{1,*} Erik L. Weerden,² Jens Eisert,^{1,3} and Yasir Iqbal⁴

¹*Freie Universität Berlin, Dahlem Center for Complex Quantum Systems
and Institut für Theoretische Physik, Arnimallee 14, 14195 Berlin, Germany*

²*University of Cologne, Institute for Theoretical Physics, Zùlpicher Straße 77, 50937 Köln, Germany*

³*Helmholtz-Zentrum Berlin für Materialien und Energie, Hahn-Meitner-Platz 1, 14109 Berlin, Germany*

⁴*Indian Institute of Technology Madras, Department of Physics and Quantum Centre of
Excellence for Diamond and Emergent Materials (QuCenDiEM), Chennai 600036, India*

The spin-1/2 Heisenberg antiferromagnet on the two-dimensional ruby and maple-leaf lattices is emerging as a new paradigmatic model of frustrated quantum magnetism, with the potential to realize intricate many-body phases on both mineral and synthetic platforms. We provide evidence that the generalized model interpolating between these two lattices features an extended quantum spin liquid ground state, which is gapless on the ruby lattice and gapped on the maple-leaf lattice, with the transition between the two occurring midway. Our results are based on one of the most extensive state-of-the-art variational infinite tensor network calculations to date, thereby helping us to resolve the long-standing issue of the delicate competition between magnetically ordered and paramagnetic states in this family of models.

Quantum spin liquids (QSLs) are complex many-body phases featuring exotic properties such as long-range entanglement and fractionalized quasi-particle excitations [1, 2]. Substantial theoretical and experimental effort is devoted in proposing model Hamiltonians and realizing such systems in the laboratory. Oftentimes, they are sought after in frustrated spin systems, where competing interactions between the spins can lead to absence of magnetic order down to zero temperature. A prominent example is the Heisenberg model on the kagome lattice, which realizes a QSL ground state with the possibility of hosting a gapped spin liquid with \mathbb{Z}_2 topological order [3–5] or a gapless $U(1)$ Dirac spin liquid [6–9].

Recently, the relatively lesser known two-dimensional ruby lattice [10] and *maple-leaf lattice* (MLL) [11] [see Fig. 1] have attracted increasing experimental and theoretical interest. The MLL is a regular 1/7 site-depleted triangular lattice with a coordination number of five (in-between that of the kagome and triangular lattices), which features three symmetry inequivalent bonds, endowing it with strong geometric frustration and enhanced quantum fluctuations for antiferromagnetic interactions. One can interpolate continuously from the MLL to the ruby lattice by tuning one of the couplings to zero, i.e., it can be viewed as a bond-depleted MLL, with a lower coordination number of four, but absence of one frustrating bond. Hence, this generalized interpolating model provides an ideal platform for hosting exotic nonmagnetic quantum many-body phases. The theoretical interest is further fueled by possible realizations of ruby lattice Hamiltonians on synthetic quantum platforms and MLL antiferromagnets in several quantum materials. Indeed, a topologically ordered QSL state has been reportedly realized on programmable quantum simulators based on Rydberg atom arrays forming a ruby lattice [12–17], while the MLL is the underlying lattice for many copper-based materials, such as spangolite [18, 19], sabelliite [20], mojaveite [21], fuetterite [22] and bluebelite [21, 23, 24], and also some semi-classical antiferromagnets like $\text{MgMn}_3\text{O}_7 \cdot 3\text{H}_2\text{O}$ [25] and $\text{Na}_2\text{Mn}_3\text{O}_7$ [26, 27].

Motivated by this state of affairs, we explore the ground state phase diagram of the ruby lattice and MLL along the entire parameter axis of the interpolating model and beyond. In this context, the central debate is whether the ground state of the isotropic Heisenberg model is a quantum paramagnet or features long-range magnetic order [10, 28–30]. While *pseudo-fermion functional renormalization group* (pf-FRG) [31] and *density-matrix renormalization group* (DMRG) together with neural network based analysis [32] identify a tiny paramagnetic regime with ordered ground states in the isotropic limits, the conclusions from coupled cluster methods [29] depend sensitively on the extrapolation scheme employed, thus highlighting the precarious nature of the magnetic fluctuation tendencies. If the former scenario prevails, the challenging question to address is whether a QSL could be realized and decipher its nature. Indeed, numerically, frustrated quantum systems pose significant technical challenges. First, the exponential many-body Hilbert space limits exact calculations to small system sizes, so approximate methods have to be used. Second, frustration typically leads to strong competition between energetically close states and complex, possibly long-range, entanglement patterns in the system. *Tensor networks* (TNs) building on area laws for entanglement entropies [33] provide a powerful toolbox for the theoretical and numerical study of quantum many-body systems [34, 35], while new method development is still undergoing. In such approaches, the quantum state is encoded in a network of local tensors, which is contracted along the virtual TN indices. Its approximation can be systematically improved with controlled tuning parameters. The two-dimensional version of TNs [36], the (infinite) *projected entangled pair state* (PEPS), has technically matured substantially in recent years due to the development of variational optimization techniques based on energy minimization [37–39]. This makes them indeed competitive with other numerical techniques, such as variational quantum Monte Carlo, density-matrix renormalization group or coupled cluster methods.

The aim of this letter is twofold: On the one hand, building on the method development of recent years, we present one of the most extensive variational PEPS studies to date, which naturally advances so-called spiral PEPS ansätze by extending them to non-Bravais lattices and finite magnetic fields, to better capture properties of frustrated quantum systems. On the other hand, motivated by the physics of the problem, we address the extremely delicate question of magnetic order in the ground state as a challenging test case. Allowing for tuning one of the couplings in the spin-1/2 Heisenberg antiferromagnetic model, we interpolate between the ruby lattice and the MLL, and beyond into the known exact dimer product phase. Our results indicate the absence of magnetic order in the ground state on the ruby lattice and MLL limits and also along the entire parameter axis interpolating between the two. We provide compelling evidence for absence of translation and point group symmetry breaking, indicating an extended QSL phase, with a previously unknown transition from a gapless to a gapped region as revealed by the width of the zero-magnetization plateau. In this context, the ruby lattice is found to host a gapless QSL while the MLL a gapped QSL.

Model and methods. We study the spin-1/2 Heisenberg model on the generalized MLL with the Hamiltonian

$$\mathcal{H} = J_r \sum_{\langle i,j \rangle_r} \mathbf{S}_i \cdot \mathbf{S}_j + J_g \sum_{\langle i,j \rangle_g} \mathbf{S}_i \cdot \mathbf{S}_j + J_b \sum_{\langle i,j \rangle_b} \mathbf{S}_i \cdot \mathbf{S}_j, \quad (1)$$

where $\langle i,j \rangle$ denotes the three types of symmetry inequivalent nearest-neighbor bonds, visualized as red, green and blue lines in Fig. 1. For simulations in the presence of an external

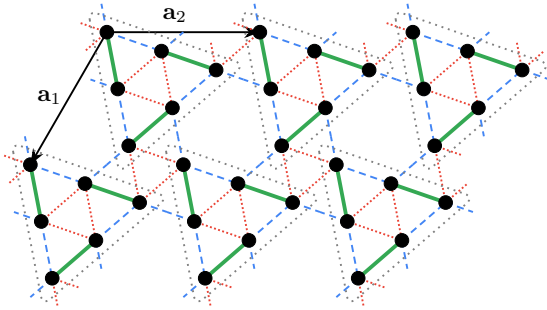


FIG. 1. Illustration of the maple-leaf lattice with the symmetry inequivalent bonds in red, green and blue. In the absence of green bonds, one obtains the ruby lattice. Both lattices have a six-site geometric unit cell basis (shown by the dotted gray triangles) with an underlying triangular Bravais lattice spanned by \mathbf{a}_1 and \mathbf{a}_2 .

magnetic field, the Hamiltonian in Eq. (1) is extended by an additional Zeeman term $-h_z \sum_i S_i^z$. We focus on the completely antiferromagnet model with two of the couplings fixed as $J_r = J_b = 1$ and varying the interaction strength J_g on green bonds. Thus our study includes both the isotropic ruby lattice ($J_g = 0$) and MLL ($J_g = 1$) limits, and tunes into the exact dimer phase for large J_g , for which spins on the

green bonds pair into singlets [40, 41]. The Heisenberg model on the MLL has previously been studied using exact diagonalization and coupled cluster methods [28–30], DMRG and neural network analyses [32, 40, 42], as well as pf-FRG [31] approaches, reaching varying conclusions. With increasing J_g , the coupled cluster method has predicted a direct transition from the six sublattice Néel antiferromagnet to the dimer product state, supported by a recent infinite DMRG [32] study, while pf-FRG [31] calculations have suggested an intermediate phase, that could possibly be a quantum paramagnet.

For the simulation of the Hamiltonian in Eq. (1), we employ TN methods in the form of two-dimensional infinite *projected entangled pair states* (PEPS). To this end, the six spins in the elementary unit cell of the MLL are coarse-grained into an effective site on a triangular lattice, spanned by lattice vectors \mathbf{a}_1 and \mathbf{a}_2 as indicated in Fig. 1. The triangular lattice is then treated as a regular square lattice with next-to-nearest neighbour interactions along the diagonal $\mathbf{a}_1 + \mathbf{a}_2$. Using the recently introduced *spiral PEPS ansatz* [43], the full many-body state vector is expressed as a network of a single PEPS tensor, together with a global unitary transformation parameterized by a wave vector $\mathbf{k} \in \mathbb{R}^2$. To obtain the ground state wave vector, the spiral PEPS ansatz is variationally optimized to find the best state approximation at bond dimension χ_B . Utilizing *automatic differentiation* as implemented in Ref. [44], an energy gradient is calculated to minimize the energy expectation value. Variational PEPS has proven to be advantageous in the study of frustrated spin systems including QSLs [45–48], where computationally cheaper methods based on imaginary time evolution can be inaccurate. For more details on the numerical setup we refer to the supplemental material [49] (see also Refs. [43, 50–56] therein).

Results. With the chosen setup of Heisenberg interactions, we map out a one-dimensional slice of the antiferromagnetic region of the phase diagram. In Fig. 2, we present the variational ground state energies per spin E_0 as a function of the coupling parameter J_g . Increasing the bulk bond dimension χ_B leads to a consistent decrease in energy, as more entanglement is captured in the system. The high-point of frustration is located in the vicinity of the isotropic MLL antiferromagnet, where E_0 reaches its maximum value and the system is least able to minimise each local Hamiltonian term simultaneously. The progressive decrease in E_0 , and hence in frustration, as J_g is lowered reflects the fact that we lose a frustrating bond as we approach the ruby lattice limit, despite its lower coordination number $z = 4$ compared to $z = 5$ for the MLL. This potentially explains the comparatively higher sensitivity of E_0 to χ_B with increasing J_g . The known exact dimer phase is found for $J_g > 1.45$ [30–32], where all simulations collapse to the analytical energy of $E_0 = -3J_g/8$, with $\langle \mathbf{S}_i \cdot \mathbf{S}_j \rangle = -3/4$ on the green bonds and zero on the red and blue bonds [see inset of Fig. 2]. At this point the system undergoes a transition from a spiral ground state (at finite χ_B) with wave vector $\mathbf{k} = (2\pi/3, 2\pi/3)$, found by varia-

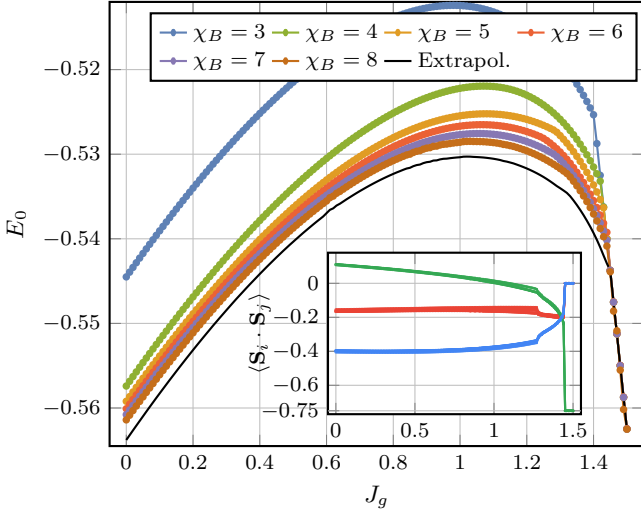


FIG. 2. Ground state energy per spin as a function of the coupling J_g for various PEPS bond dimensions χ_B . The linear slope for $J_g > 1.45$ is given by $E_0 = -3J_g/8$, i.e., the energy of the exact dimer state. The inset shows the individual bond energies $\langle \mathbf{S}_i \cdot \mathbf{S}_j \rangle$ for the fifteen different nearest-neighbour bonds in the MLL unit cell, colored according to the three inequivalent types of bond in the lattice (cf. Fig. 1). We observe an approximate 120° rotational symmetry.

tional optimization, to a fully translational invariant state with $\mathbf{k} = (0, 0)$. In order to determine the infinite bond dimension limit, i.e., $E_0(\chi_B \rightarrow \infty)$, we employ an extrapolation procedure as described in the SM [57] (see also Refs. [8, 58–62] therein), yielding

$$\begin{aligned} E_0(\text{Ruby}) &= -0.5639(20), \\ E_0(\text{MLL}) &= -0.5304(25). \end{aligned} \quad (2)$$

Note, that while the resulting black line in Fig. 2 provides a meaningful energy, it is not a true upper bound in a variational sense.

The ground state energy shows an additional kink, indicating another transition beyond the one to the exact dimer phase. To resolve the phase diagram of the model and address the potential presence or absence of magnetic order, we analyze the magnetic order parameter, given by the average staggered magnetization per spin

$$m^2 = \frac{1}{N} \sum_{i=1}^N (\langle S_i^x \rangle^2 + \langle S_i^y \rangle^2 + \langle S_i^z \rangle^2). \quad (3)$$

The results are shown in Fig. 3. Reflecting the behaviour of the ground state energy, the transition to the exact dimer phase is correctly captured, with a vanishing order parameter for the global singlet state. For the remaining part of the phase diagram, we can further identify two distinct regions. First, we focus on the magnetically ordered phase (a six sublattice Néel state with an eighteen site magnetic unit cell [28]) just before the transition to the dimer phase. Here, the order parameter shows a monotonic decrease with increasing χ_B , which, how-

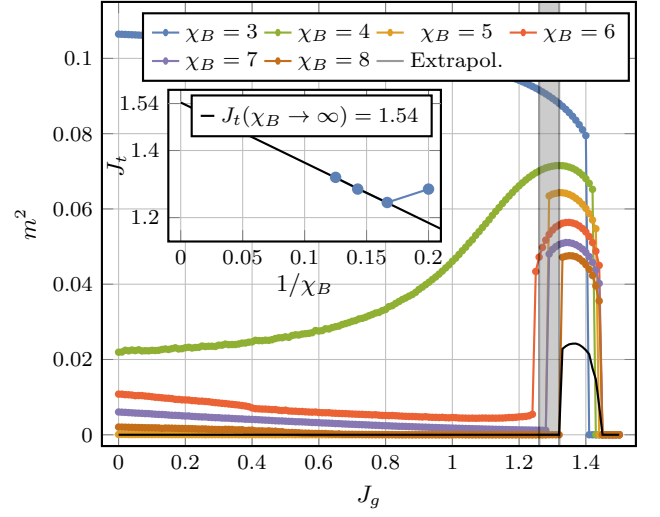


FIG. 3. Staggered magnetization of the ground state as a function of the coupling J_g for various PEPS bond dimensions χ_B . The inset shows the transition point J_t from the non-magnetic into the magnetically ordered phase in relation to the inverse bond dimension. The window of uncertainty is highlighted in gray in the main plot. Additionally, in the inset the extrapolation of the transition point J_t for $\chi_B = \{6, 7, 8\}$ to infinite bond dimension is shown.

ever, extrapolates to a finite value for infinite bond dimension (see SM [57]).

In contrast, our infinite PEPS study reveals a previously unreported quantum paramagnetic phase spanning an extended region of the phase diagram, encompassing both the isotropic ruby lattice and MLL. Interestingly, its exotic properties seem to be reflected in rather atypical TN simulation behavior, as the order parameter does not follow a monotonic behaviour with increasing bond dimension. For small bond dimensions the system remains fully ordered until it transitions to the exact dimer phase. However, for larger χ_B , the picture changes significantly, particularly at $\chi_B = 5$, where the order parameter is nearly zero throughout. Although bond dimensions $\chi_B = \{6, 7, 8\}$ again yield a finite, but small order parameters (which is also nearly zero for $\chi_B = 8$), an extrapolation of the data points (m^2 vs. $1/\chi_B$, $\chi_B \rightarrow \infty$) confirms the non-magnetic character of the ground state for $0 \leq J_g \leq 1.28$ [57]. Such a scenario has been discussed previously in a coupled cluster study [29] for $J_g = 0$ and $J_g = 1$ [29], where depending on the choice of the empirical extrapolation schemes used, the magnetic order parameter either vanishes or remains small but finite, highlighting a delicate competition. Our results should be contrasted with those of some other numerical approaches [31, 32], which suggest a Néel ordered ground state along most of the J_g axis, with only a narrow window for possible quantum disordered behavior between the dimer product and Néel orders. These distinct conclusions are likely rooted in the subtle interplay between short-distance and long-range correlations, and how these are accounted for numerically, as well as finite size effects that can bias related one-dimensional methods [63].

Inspecting the spin-spin correlations on all MLL bonds reveals a strong six-fold rotational symmetry in the ground states, as shown in the inset of Fig. 2. One can argue that this finding is striking, given that the PEPS does not enforce any point group symmetry of the lattice and furthermore distorts its $p6$ symmetry by the coarse-graining to a square lattice. The observed rotational symmetry, combined with the six-site translational symmetry in the spiral PEPS ansatz, suggests that the non-magnetic region is likely a fully symmetric QSL, respecting the $p6$ wallpaper group.

The transition point J_t from the QSL to the putative ordered phase depends on the bond dimension, as shown in the inset of Fig. 3. Given the limited available data points χ_B , we cannot draw definitive conclusions about its precise location and presence. Taking into account only the three largest values and using a linear fit in the inverse bond dimension, the transition point is extrapolated to $J_t(\chi_B \rightarrow \infty) = 1.54$, which is already in the exact dimer phase. While the transition into this phase is found at $J_g = 1.45$, consistent with previous studies [32], the fit could indicate that the magnetically ordered phase does not survive in the infinite bond dimension limit. In this case, the anisotropic Heisenberg model on the MLL would have a direct transition from the presumptive QSL into an exact dimer phase.

The presumptive QSL phase shows a slightly non-uniform convergence behaviour for the magnetic order parameter, separating the two special points of the isotropic ruby lattice and MLL. One question that naturally arises is whether this is a single connected phase or possibly composed of several different ones. The connectivity of this phase is now further analysed by assessing the effects of a magnetic field. To this end, we performed simulations with an external magnetic field for $0 \leq J_g \leq 1$ and $0 \leq h_z \leq 0.15$ at bond dimension $\chi_B = 5$. This bond dimension is chosen due to the uniform non-magnetic region and the trade-off between accuracy and computational effort. Although the magnetic field only leads to a remaining $U(1)$ symmetry in the Hamiltonian, the spiral PEPS ansatz can still be employed by choosing the rotation axis along the direction of the field [49]. First, by focusing on the isotropic ruby lattice and MLL, we find a significantly different behaviour for small values of the field, which are shown in Fig. 4. For the ruby lattice, an immediate susceptibility to the field is observed, while there is a significant zero-magnetization plateau for the MLL. The findings strongly indicate a gapless QSL on the ruby lattice, and a gapped QSL on the MLL with a gap of $\Delta \sim 0.10$ as estimated from the width of the plateau. By scanning the different couplings J_g between those two limits, we are able to determine the transition between those regions. Results for the width of the zero-magnetization plateau Δ are shown in the inset of Fig. 4, which reveal the transition between the gapless and gapped QSL candidates to happen at $J_{t,1} \sim 0.50$. Here, the threshold to determine the plateau width is set to $m_z/m_S = 5e-7$. Although it is possible that larger χ_B could slightly shift this point, the general feature is however expected to appear.

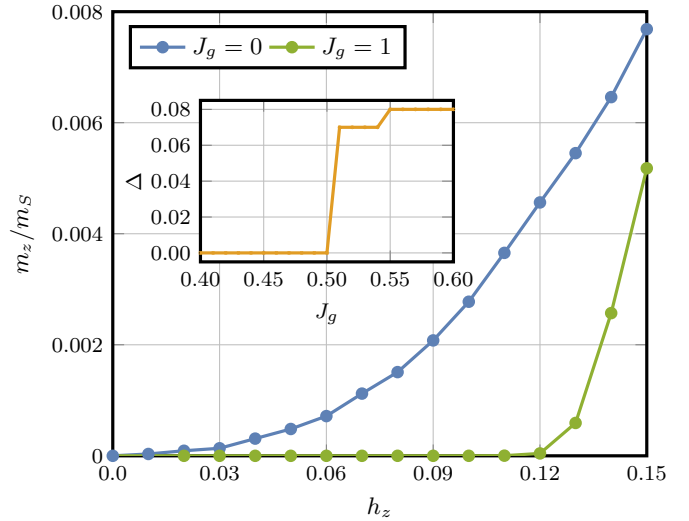


FIG. 4. Average spin component $m_z = \langle S_z \rangle$ normalized to the saturation value $m_S = 1/2$ for the isotropic ruby lattice and MLL at $\chi_B = 5$. The ruby lattice is immediately susceptible to the magnetic field, indicating a gapless ground state. In contrast, the MLL shows a significant magnetization plateau, identifying a gapped spectrum. The inset shows the spin gap Δ as a function of J_g , revealing the transition from the gapless to a gapped region.

Conclusion and outlook. In this work we have presented an infinite two-dimensional TN study of the $S = 1/2$ Heisenberg antiferromagnet on the highly frustrated ruby and maple-leaf lattices. Using sophisticated variational energy optimization techniques, the projected entangled pair state ansatz is able to handle the challenging amount of frustration and allows us to resolve the delicate competition between magnetic order and paramagnetic tendencies in the system. Our results reveal an extended quantum paramagnetic ground state in the generalized phase diagram of the model, which interpolates between the two lattices. We do not observe any sign of lattice symmetry breaking, thus lending support to a fully symmetric QSL phase. Importantly, this phase contains the two special points for the isotropic ruby lattice and the MLL. Further decomposition of the connectivity of the putative QSL phase across the lattices reveals a fascinating quantum phase transition from a gapless region for $0 \leq J_g \leq 0.5$ to a gapped region for $0.5 < J_g \leq 1.3$, as indicated by the width of the zero-magnetization plateau. Our study thus suggests a possible resolution to the long-standing controversial issue, indicating the presence of more than one spin liquid phase. The previously reported Néel ordered phase is indeed found in the PEPS simulations, but its presence in the infinite bond dimension limit cannot be fully resolved. However, the limited finite bond dimension data seem to indicate a direct transition from a gapped paramagnet to the gapped exact dimer phase, without any intermediate ordered phase. The substantial differences with previous matrix-product wave function based studies [32] can be attributed to finite size effects, which are practically absent in our study.

As the MLL sites are not one of the “irreducible Wyckoff positions” (i.e., not centers of rotations or mirrors) there is no Lieb-Schultz-Mattis theorem associated with the MLL [64], implying that a featureless paramagnet is in principle allowed on this lattice. Our work thus sets the stage for characterizing the nature of the gapped paramagnet to ascertain whether it is a \mathbb{Z}_2 topologically ordered QSL. This would involve a calculation of the topological entanglement entropy and/or modular S and T matrices. An alternative route towards ascertaining the low-energy gauge theory of the putative QSL phase would involve a Gutzwiller projected wave function study of the energetics of recently classified \mathbb{Z}_2 QSLs [65]. Our work also calls for a classification of QSLs on the ruby lattice to assess the issue of whether the putative gapped QSL can be viewed as a pairing instability of the gapless QSL. In the scenario, that the MLL ground state is a featureless paramagnet, it will be interesting to attempt an analytical construction of this state.

The two-dimensional ruby lattice and MLL are currently developing into new paradigmatic models for realizing frustrated quantum antiferromagnetism on Rydberg atom array and quantum material platforms, respectively. As such, they pose significant challenges to numerical simulation techniques, so that as a benchmarking model they can be considered on a par with the enigmatic Kagome Heisenberg model. In this respect, our infinite two-dimensional TN results present a cornerstone in the numerical simulation of the frustrated MLL. It would also be interesting to bring the simulations closer together with material realizations with such a structure, e.g., by including longer range interactions or interactions of different types. In addition, thermodynamic properties are readily accessible in the TN formalism [66].

Simulations. The numerical simulation were performed using the publicly available *variPEPS* library in version 0.6.0 [67], as presented in Ref. [44].

CO₂-emissions table. The TN calculations in this work demanded significant computational resources. To highlight the environmental impact, Table I shows a conservative estimate of the carbon emissions from these simulations, advocating for greater carbon footprint awareness in numerical research.

TN simulations	
Total kernel time	~ 5.3 million h
Thermal design power per kernel	12 W
Total energy consumption	~ 64 MW h
Average emission of CO ₂ in Germany in 2023 [68]	0.38 kg/kW h
Total CO ₂ emission	$\sim 24\,200$ kg
Were the emissions offset?	yes

TABLE I. Estimate of the carbon emissions produced by the numerical simulations in this work, calculated according to the Scientific CO₂nduct project [69].

Acknowledgments. We acknowledge inspiring discussions with L. Balents, S. Bhattacharjee, A. Haller, F. Krein, A. Läuchli, C. Liu, A. Nevidomskyy, A. Nietner, S. Parameswaran, K. Penc, and A. Wietek. This work has been funded by the Deutsche Forschungsgemeinschaft (DFG, German Research Foundation) under the project number 277101999 – CRC 183 (project B01), and the BMBF (MUNIQ-Atoms, FermiQP). P. S. and J. N. thank the ZEDV (IT support) of the physics department, Freie Universität Berlin, for computing time and their technical support, particularly we thank J. Behrmann, C. Hoffmann and J. Dreger. We also acknowledge the computing time provided by the HPC Service of FUB-IT, Freie Universität Berlin [70]. J. E. acknowledges funding of the ERC (DebuQC). The work of Y. I. was performed in part at the Aspen Center for Physics, which is supported by National Science Foundation Grant No. PHY-2210452. The participation of Y. I. at the Aspen Center for Physics was supported by the Simons Foundation. The research of Y. I. was carried out, in part, at the Kavli Institute for Theoretical Physics in Santa Barbara during the “A New Spin on Quantum Magnets” program in summer 2023 and “Correlated Gapless Quantum Matter” program in spring 2024, supported by the National Science Foundation under Grant No. NSF PHY-1748958. Y. I. thanks the Pollica Physics Centre for the workshop “Exotic quantum matter from quantum spin liquids to novel field theories” where this manuscript was completed. Y. I. acknowledges support from the ICTP through the Associates Programme, from the Simons Foundation through Grant No. 284558FY19, and IIT Madras through the Institute of Eminence (IoE) program for establishing QuCenDiEM (Project No. SP22231244CPETWOQCDHOC). Y. I. also acknowledges the use of the computing resources at HPCE, IIT Madras.

* Both authors contributed equally.

- [1] L. Balents, Spin liquids in frustrated magnets, *Nature* **464**, 199 (2010).
- [2] L. Savary and L. Balents, Quantum spin liquids: a review, *Rep. Prog. Phys.* **80**, 016502 (2016).
- [3] S. Yan, D. A. Huse, and S. R. White, Spin-liquid ground state of the $S = 1/2$ kagome Heisenberg antiferromagnet, *Science* **332**, 1173 (2011).
- [4] S. Depenbrock, I. P. McCulloch, and U. Schollwöck, Nature of the spin-liquid ground state of the $S = 1/2$ Heisenberg model on the Kagome lattice, *Phys. Rev. Lett.* **109**, 067201 (2012).
- [5] A. M. Läuchli, J. Sudan, and R. Moessner, $S = \frac{1}{2}$ kagome Heisenberg antiferromagnet revisited, *Phys. Rev. B* **100**, 155142 (2019).
- [6] Y. Iqbal, F. Becca, S. Sorella, and D. Poilblanc, Gapless spin-liquid phase in the kagome spin- $\frac{1}{2}$ Heisenberg antiferromagnet, *Phys. Rev. B* **87**, 060405 (2013).
- [7] Y. Iqbal, D. Poilblanc, and F. Becca, Vanishing spin gap in a competing spin-liquid phase in the kagome Heisenberg antiferromagnet, *Phys. Rev. B* **89**, 020407 (2014).
- [8] H. J. Liao, Z. Y. Xie, J. Chen, Z. Y. Liu, H. D. Xie, R. Z. Huang, B. Normand, and T. Xiang, Gapless spin-liquid ground state in

- the $S = 1/2$ Kagome antiferromagnet, *Phys. Rev. Lett.* **118**, 137202 (2017).
- [9] Y.-C. He, M. P. Zaletel, M. Oshikawa, and F. Pollmann, Signatures of Dirac cones in a DMRG study of the kagome Heisenberg Model, *Phys. Rev. X* **7**, 031020 (2017).
- [10] J. Richter, J. Schulenburg, and A. Honecker, Quantum magnetism in two dimensions: From semi-classical néel order to magnetic disorder, in *Quantum Magnetism*, edited by U. Schollwöck, J. Richter, D. J. J. Farnell, and R. F. Bishop (Springer Berlin Heidelberg, Berlin, Heidelberg, 2004) pp. 85–153.
- [11] D. Betts, A new two-dimensional lattice of coordination number five, *Proc. N. S. Inst. Sci.* **40**, 95 (1995).
- [12] G. Semeghini, H. Levine, A. Keesling, S. Ebadi, T. T. Wang, D. Bluvstein, R. Verresen, H. Pichler, M. Kalinowski, R. Samajdar, A. Omran, S. Sachdev, A. Vishwanath, M. Greiner, V. Vuletić, and M. D. Lukin, Probing topological spin liquids on a programmable quantum simulator, *Science* **374**, 1242 (2021).
- [13] R. Verresen, M. D. Lukin, and A. Vishwanath, Prediction of toric code topological order from Rydberg blockade, *Phys. Rev. X* **11**, 031005 (2021).
- [14] G. Giudici, M. D. Lukin, and H. Pichler, Dynamical preparation of quantum spin liquids in Rydberg atom arrays, *Phys. Rev. Lett.* **129**, 090401 (2022).
- [15] R. Verresen and A. Vishwanath, Unifying Kitaev magnets, kagomé dimer models, and ruby Rydberg spin liquids, *Phys. Rev. X* **12**, 041029 (2022).
- [16] A. W. Glaetzle, M. Dalmonte, R. Nath, I. Rousochatzakis, R. Moessner, and P. Zoller, Quantum spin-ice and dimer models with Rydberg atoms, *Phys. Rev. X* **4**, 041037 (2014).
- [17] R. Samajdar, D. G. Joshi, Y. Teng, and S. Sachdev, Emergent \mathbb{Z}_2 gauge theories and topological excitations in Rydberg atom arrays, *Phys. Rev. Lett.* **130**, 043601 (2023).
- [18] F. C. Hawthorne, M. Kimata, and R. K. Eby, The crystal structure of spangolite, a complex copper sulfate sheet mineral, *Am. Mineral.* **78**, 649 (1993).
- [19] P. Schmoll, H. O. Jeschke, and Y. Iqbal, Tensor network analysis of the maple-leaf antiferromagnet spangolite (2024), [arXiv:2404.14905](https://arxiv.org/abs/2404.14905).
- [20] F. Olmi, C. Sabelli, and R. Trosti-Ferroni, The crystal structure of sabelliite, *Eur. J. Mineral.* **7**, 1331 (1995).
- [21] S. J. Mills, A. R. Kampf, A. G. Christy, R. M. Housley, G. R. Rossman, R. E. Reynolds, and J. Marty, Bluebellite and mojaveite, two new minerals from the central Mojave desert, California, USA, *Mineralog. Mag.* **78**, 1325–1340 (2014).
- [22] A. R. Kampf, S. J. Mills, R. M. Housley, and J. Marty, Lead-tellurium oxysalts from Otto Mountain near Baker, California: VIII. Fuettererite, $\text{Pb}_3\text{Cu}_6^{2+}\text{Te}_6^{6+}\text{O}_6(\text{OH})_7\text{Cl}_5$, a new mineral with double spangolite-type sheets, *Am. Mineralog.* **98**, 506 (2013).
- [23] R. Makuta and C. Hotta, Dimensional reduction in quantum spin- $\frac{1}{2}$ system on a $\frac{1}{7}$ -depleted triangular lattice, *Phys. Rev. B* **104**, 224415 (2021).
- [24] P. Ghosh, T. Müller, Y. Iqbal, R. Thomale, and H. O. Jeschke, Effective spin-1 breathing kagome Hamiltonian induced by the exchange hierarchy in the maple leaf mineral bluebellite, *Phys. Rev. B* **110**, 094406 (2024).
- [25] Y. Haraguchi, A. Matsuo, K. Kindo, and Z. Hiroi, Frustrated magnetism of the maple-leaf-lattice antiferromagnet $\text{MgMn}_3\text{O}_7 \cdot 3\text{H}_2\text{O}$, *Phys. Rev. B* **98**, 064412 (2018).
- [26] C. Venkatesh, B. Bandyopadhyay, A. Midya, K. Mahalingam, V. Ganesan, and P. Mandal, Magnetic properties of the one-dimensional $S = \frac{3}{2}$ Heisenberg antiferromagnetic spin-chain compound $\text{Na}_2\text{Mn}_3\text{O}_7$, *Phys. Rev. B* **101**, 184429 (2020).
- [27] B. Saha, A. K. Bera, S. M. Yusuf, and A. Hoser, Two-dimensional short-range spin-spin correlations in the layered spin- $\frac{3}{2}$ maple leaf lattice antiferromagnet $\text{Na}_2\text{Mn}_3\text{O}_7$ with crystal stacking disorder, *Phys. Rev. B* **107**, 064419 (2023).
- [28] D. Schmalzfuß, P. Tomczak, J. Schulenburg, and J. Richter, The spin- $\frac{1}{2}$ Heisenberg antiferromagnet on a $\frac{1}{7}$ -depleted triangular lattice: Ground-state properties, *Phys. Rev. B* **65**, 224405 (2002).
- [29] D. J. J. Farnell, O. Götze, J. Richter, R. F. Bishop, and P. H. Y. Li, Quantum $s = \frac{1}{2}$ antiferromagnets on Archimedean lattices: The route from semiclassical magnetic order to nonmagnetic quantum states, *Phys. Rev. B* **89**, 184407 (2014).
- [30] D. J. J. Farnell, R. Darradi, R. Schmidt, and J. Richter, Spin-half Heisenberg antiferromagnet on two archimedean lattices: From the bounce lattice to the maple-leaf lattice and beyond, *Phys. Rev. B* **84**, 104406 (2011).
- [31] L. Gresista, C. Hickey, S. Trebst, and Y. Iqbal, Candidate quantum disordered intermediate phase in the Heisenberg antiferromagnet on the maple-leaf lattice, *Phys. Rev. B* **108**, L241116 (2023).
- [32] J. Beck, J. Bodky, J. Motruk, T. Müller, R. Thomale, and P. Ghosh, Phase diagram of the $J-J_d$ Heisenberg model on the maple leaf lattice: Neural networks and density matrix renormalization group, *Phys. Rev. B* **109**, 184422 (2024).
- [33] J. Eisert, M. Cramer, and M. B. Plenio, Area laws for the entanglement entropy, *Rev. Mod. Phys.* **82**, 277 (2010).
- [34] R. Orús, Tensor networks for complex quantum systems, *Nature Rev. Phys.* **1**, 538 (2019).
- [35] J. I. Cirac, D. Pérez-García, N. Schuch, and F. Verstraete, Matrix product states and projected entangled pair states: Concepts, symmetries, theorems, *Rev. Mod. Phys.* **93**, 045003 (2021).
- [36] F. Verstraete and J. I. Cirac, Renormalization algorithms for quantum-many body systems in two and higher dimensions (2004), [arXiv:cond-mat/0407066](https://arxiv.org/abs/cond-mat/0407066).
- [37] P. Corboz, Variational optimization with infinite projected entangled-pair states, *Phys. Rev. B* **94**, 035133 (2016).
- [38] L. Vanderstraeten, J. Haegeman, P. Corboz, and F. Verstraete, Gradient methods for variational optimization of projected entangled-pair states, *Phys. Rev. B* **94**, 155123 (2016).
- [39] H.-J. Liao, J.-G. Liu, L. Wang, and T. Xiang, Differentiable programming tensor networks, *Phys. Rev. X* **9**, 031041 (2019).
- [40] P. Ghosh, T. Müller, and R. Thomale, Another exact ground state of a two-dimensional quantum antiferromagnet, *Phys. Rev. B* **105**, L180412 (2022).
- [41] G. Misguich, C. Lhuillier, B. Bernu, and C. Waldtmann, Spin-liquid phase of the multiple-spin exchange Hamiltonian on the triangular lattice, *Phys. Rev. B* **60**, 1064 (1999).
- [42] P. Ghosh, Where is the spin liquid in maple-leaf quantum magnet? (2024), [arXiv:2401.09422](https://arxiv.org/abs/2401.09422).
- [43] J. Hasik and P. Corboz, Incommensurate order with translationally invariant projected entangled-pair states: Spiral states and quantum spin liquid on the anisotropic triangular lattice, *Phys. Rev. Lett.* **133**, 176502 (2024).
- [44] J. Naumann, E. L. Weerden, M. Rizzi, J. Eisert, and P. Schmoll, An introduction to infinite projected entangled-pair state methods for variational ground state simulations using automatic differentiation, *SciPost Phys. Lect. Notes*, 86 (2024).
- [45] J. Hasik, D. Poilblanc, and F. Becca, Investigation of the Néel phase of the frustrated Heisenberg antiferromagnet by differentiable symmetric tensor networks, *SciPost Phys.* **10**, 012 (2021).
- [46] J. Hasik, M. Van Damme, D. Poilblanc, and L. Vanderstraeten, Simulating chiral spin liquids with projected entangled-pair states, *Phys. Rev. Lett.* **129**, 177201 (2022).

- [47] S. Niu, J. Hasik, J.-Y. Chen, and D. Poilblanc, Chiral spin liquids on the kagome lattice with projected entangled simplex states, *Phys. Rev. B* **106**, 245119 (2022).
- [48] X.-Y. Zhang, S. Liang, H.-J. Liao, W. Li, and L. Wang, Differentiable programming tensor networks for Kitaev magnets, *Phys. Rev. B* **108**, 085103 (2023).
- [49] See Section “Spiral PEPS setup for the maple-leaf lattice” in the Supplemental Material at [URL], which includes Refs. [43, 50–56].
- [50] P. Silvi, F. Tschirsich, M. Gerster, J. Jünemann, D. Jaschke, M. Rizzi, and S. Montangero, The tensor networks anthology: Simulation techniques for many-body quantum lattice systems, *SciPost Phys. Lect. Notes*, **8** (2019).
- [51] P. Scholl, S. Singh, M. Rizzi, and R. Orús, A programming guide for tensor networks with global $SU(2)$ symmetry, *Ann. Phys.* **419**, 168232 (2020).
- [52] A. V. Chubukov, On the quantum effects in helimagnets, *J. Phys. C* **17**, L991 (1984).
- [53] Y. Iqbal, P. Ghosh, R. Narayanan, B. Kumar, J. Reuther, and R. Thomale, Intertwined nematic orders in a frustrated ferromagnet, *Phys. Rev. B* **94**, 224403 (2016).
- [54] T. Nishino and K. Okunishi, Corner transfer matrix renormalization group method, *J. Phys. Soc. Jpn.* **65**, 891 (1996).
- [55] T. Nishino and K. Okunishi, Corner transfer matrix algorithm for classical renormalization group, *J. Phys. Soc. Jpn.* **66**, 3040 (1997).
- [56] R. Orús and G. Vidal, Simulation of two-dimensional quantum systems on an infinite lattice revisited: Corner transfer matrix for tensor contraction, *Phys. Rev. B* **80**, 094403 (2009).
- [57] See Section “Finite bond dimension extrapolation” in the Supplemental Material at [URL], which includes Refs. [8, 58–62].
- [58] P. Corboz, P. Czarnik, G. Kapteijns, and L. Tagliacozzo, Finite correlation length scaling with infinite projected entangled-pair states, *Phys. Rev. X* **8**, 031031 (2018).
- [59] M. Rader and A. M. Läuchli, Finite correlation length scaling in Lorentz-invariant gapless iPEPS wave functions, *Phys. Rev. X* **8**, 031030 (2018).
- [60] B. Vanhecke, J. Hasik, F. Verstraete, and L. Vanderstraeten, Scaling hypothesis for projected entangled-pair states, *Phys. Rev. Lett.* **129**, 200601 (2022).
- [61] B. Pirvu, G. Vidal, F. Verstraete, and L. Tagliacozzo, Matrix product states for critical spin chains: Finite-size versus finite-entanglement scaling, *Phys. Rev. B* **86**, 075117 (2012).
- [62] P. Corboz, Improved energy extrapolation with infinite projected entangled-pair states applied to the two-dimensional hubbard model, *Phys. Rev. B* **93**, 045116 (2016).
- [63] E. L. Weerden and M. Rizzi, Fractional quantum Hall states with variational projected entangled-pair states: A study of the bosonic Harper-Hofstadter model, *Phys. Rev. B* **109**, L241117 (2024).
- [64] H. C. Po, H. Watanabe, C.-M. Jian, and M. P. Zaletel, Lattice Homotopy Constraints on Phases of Quantum Magnets, *Phys. Rev. Lett.* **119**, 127202 (2017).
- [65] J. Sonnenschein, A. Maity, C. Liu, R. Thomale, F. Ferrari, and Y. Iqbal, Candidate quantum spin liquids on the maple-leaf lattice (2024), [arXiv:2404.05617](https://arxiv.org/abs/2404.05617).
- [66] P. Scholl, C. Balz, B. Lake, J. Eisert, and A. Kshetrimayum, Finite temperature tensor network algorithm for frustrated two-dimensional quantum materials, *Phys. Rev. B* **109**, 235119 (2024).
- [67] J. Naumann, P. Scholl, F. Wilde, and F. Krein, *variPEPS (Python version)* (0.6.0), Zenodo (2024).
- [68] P. Icha and T. Lauf, *Entwicklung der spezifischen Treibhausgas-Emissionen des deutschen Strommix in den Jahren 1990 - 2023*, Climate Change No. 23/2024 (Umweltbundesamt, 2024).
- [69] R. Sweke, P. Boes, N. Ng, C. Sparaciari, J. Eisert, and M. Gohl, Transparent reporting of research-related greenhouse gas emissions through the scientific CO2nduct initiative, *Comm. Phys.* **5**, 150 (2022).
- [70] L. Bennett, B. Melchers, and B. Proppe, *Curta: A General-purpose High-Performance Computer at ZEDAT, Freie Universität Berlin* (2020).
- [71] P. Corboz, Variational optimization with infinite projected entangled-pair states, *Phys. Rev. B* **94**, 035133 (2016).
- [72] B. Ponsioen and P. Corboz, Excitations with projected entangled pair states using the corner transfer matrix method, *Phys. Rev. B* **101**, 195109 (2020).
- [73] B. Ponsioen, J. Hasik, and P. Corboz, Improved summations of n -point correlation functions of projected entangled-pair states, *Phys. Rev. B* **108**, 195111 (2023).
- [74] W.-L. Tu, L. Vanderstraeten, N. Schuch, H.-Y. Lee, N. Kawashima, and J.-Y. Chen, Generating function for projected entangled-pair states, *PRX Quantum* **5**, 010335 (2024).

Spiral PEPS setup for the maple-leaf lattice

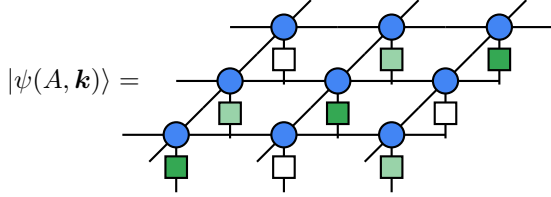
Variational PEPS simulations of the maple-leaf lattice are performed using the spiral PEPS ansatz [43]. The full many-body state vector

$$|\psi(A, \mathbf{k})\rangle = U(\mathbf{k}) \sum_{\{s_i\}} C_{\{s_i\}}(A) |\{s_i\}\rangle \quad (4)$$

is expressed as a network of a single tensor A , mapping from parameter space to the physical amplitudes by $C_{\{s_i\}}(A)$, together with a global unitary transformation parameterized by a wave vector $\mathbf{k} \in \mathbb{R}^2$. The global unitary transformation can be decomposed into a product of spatially dependent local unitaries as

$$U(\mathbf{k}) = \prod_{\mathbf{r}} u_{\mathbf{r}}(\mathbf{k}) \quad (5)$$

that act only on the combined physical index of the six spins. The full infinite spiral PEPS state vector is then given by



One advantage of this approach is that for models with a global symmetry such as $SU(2)$, arbitrary unit cells can be generated by only a single-site tensor and corresponding relative rotations. This is computationally more efficient than choosing a large unit cell of different tensors and allows us to reach notably large bond dimensions, given no global symmetries are exploited in the TN [50, 51]. Moreover, the spiral pitch vector of the magnetically ordered state can be variationally optimized together with the PEPS tensor [43], such that the ansatz faithfully represents the structure of the target state. This is important because quantum fluctuations lead to a shift of the spiral pitch vector and the relative angle between spins in the unit cell compared to their classical values [52, 53]. The tensor A has four virtual indices with a bulk bond dimension χ_B , as well as a physical index of dimension $d = 2^6$ due to the chosen coarse-graining. To this end, the basis of six spins is coarse-grained into an effective PEPS site, which introduces next-to-nearest neighbour interactions on the resulting square lattice. In order to contract the infinite TN for the calculation of its norm and expectation values, we employ a regular *corner transfer matrix renormalization group* (CTMRG) scheme [54–56]. It calculates fixed-point environment tensors using an iterative power method. The unavoidable approximations in this procedure are controlled by an additional refinement parameter, the environment bond dimension χ_E . In all simulations, χ_E is chosen to be sufficiently high for the results to be converged, or as the largest value for computational feasibility.

For the labeling convention of the MLL, the two basis vectors are given by

$$\mathbf{a}_1 = -\frac{\sqrt{7}}{2} \begin{pmatrix} 1 \\ \sqrt{3} \end{pmatrix} \quad \mathbf{a}_2 = \sqrt{7} \begin{pmatrix} 1 \\ 0 \end{pmatrix}. \quad (6)$$

Here, the lattice constant is set to $a = 1$. For the spiral PEPS ansatz on the square lattice, we map these vectors to the orthonormal vectors $\mathbf{a}_1 \mapsto -\hat{e}_y$ and $\mathbf{a}_2 \mapsto +\hat{e}_x$. The spiral is then defined collectively for the six-site basis, still parametrized by a single two-dimensional wave vector $\mathbf{k} \in \mathbb{R}^2$. It is incorporated into the calculation of expectation values of vertical, horizontal and diagonal interactions on the square lattice. It is advantageous to choose the spiral rotation around the y -axis, which allows one to work entirely in the xz -plane. Here, a PEPS ansatz with purely real tensor coefficients can be used [43], which reduces the computation cost. The local unitary transformations on site \mathbf{r} are then given by

$$u_{\mathbf{r}}(\mathbf{k}, \mathbf{r}') = \exp[i\pi(\mathbf{k} \cdot \mathbf{r}') S_{\mathbf{r}'}^y]. \quad (7)$$

Due to the $SU(2)$ symmetry of the Heisenberg Hamiltonian, its action on the interaction terms only depend on the relative position of the coarse-grained sites involved, so that we have $\mathbf{r}' = \mathbf{a}_1$, $\mathbf{r}' = \mathbf{a}_2$ and $\mathbf{r}' = \mathbf{a}_1 + \mathbf{a}_2$ for the three types of interactions (vertical, horizontal and diagonal). The eighteen site unit cell of the classical ground state then corresponds to a wave vector $\mathbf{k} = (2\pi/3, 2\pi/3)$ on the coarse-grained square lattice. This is also the structure we found by numerically optimizing over \mathbf{k} for the ground state outside the exact dimer phase. Note that if the structure of the ground state is known, a fixed wave vector \mathbf{k} can also be imprinted, leaving only the bulk PEPS tensor to be variationally optimized.

When including an external magnetic field, the Hamiltonian only possesses a $U(1)$ symmetry. Fortunately, the spiral PEPS ansatz can still be used with a rotation around the axis of the field. However, in contrast to the $SU(2)$ -symmetric Hamiltonian, now a PEPS tensor with complex coefficients needs to be chosen. The wave vector can be optimized to find the correct structure for the ground states, which allows the spiral PEPS ansatz to capture the correct pattern for magnetization plateaus, as for instance found for the isotropic Heisenberg model on the maple-leaf lattice at $\langle S_z \rangle = 0$. The basis of the

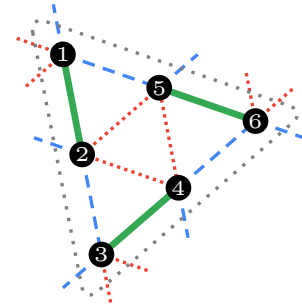


FIG. 5. Definition of one unit cell, the six-site basis of the maple-leaf lattice.

maple-leaf lattice is defined in Fig. 5. In the translational invariant spiral PEPS ansatz there are only six individual spins, and fifteen different nearest-neighbour bonds in the network. The unit cell sites are spanned by the following six basis vectors

$$\begin{aligned} \mathbf{b}_1 &= \begin{pmatrix} 0 \\ 0 \end{pmatrix}, & \mathbf{b}_4 &= \frac{1}{\sqrt{7}} \begin{pmatrix} 3 \\ -2\sqrt{3} \end{pmatrix}, \\ \mathbf{b}_2 &= \frac{1}{2\sqrt{7}} \begin{pmatrix} 1 \\ -3\sqrt{3} \end{pmatrix}, & \mathbf{b}_5 &= \frac{1}{2\sqrt{7}} \begin{pmatrix} 5 \\ -\sqrt{3} \end{pmatrix}, \\ \mathbf{b}_3 &= \frac{1}{\sqrt{7}} \begin{pmatrix} 1 \\ -3\sqrt{3} \end{pmatrix}, & \mathbf{b}_6 &= \frac{1}{\sqrt{7}} \begin{pmatrix} 5 \\ -\sqrt{3} \end{pmatrix}. \end{aligned} \quad (8)$$

Those basis vectors do not enter in the unitary transformation of the spiral PEPS ansatz, as it only depends on the two-dimensional wave vector \mathbf{k} . However, they are important in the calculation of structure factors, as described below.

Virtual \mathbb{Z}_2 symmetry in the PEPS simulations

Tensor networks provide a significant advantage in numerical simulations by allowing the incorporation of global symmetries. Each tensor index is assigned quantum numbers corresponding to the underlying symmetry group, with internal couplings dictated by the appropriate fusion rules. This results in a sparse block structure for each tensor, effectively reducing the number of variational parameters in the ansatz. While this generally leads to improvements in the computational cost, it also allows to target specific symmetry sectors for the overall wave function, and thereby a symmetry-resolved analysis.

Hinting at the potential quantum spin liquid ground state for the Heisenberg model on the isotropic maple-leaf lattice, here we want to exploit the \mathbb{Z}_2 symmetry in the variational PEPS simulations. Each tensor index, typically associated with a complex vector space $\mathbb{V} = \mathbb{C}^a$, where $a = [p^6, \chi_B, \chi_E]$ in our simulations, is now represented as

$$\mathbb{V} = \bigoplus_{q=\{0,1\}} d_q \mathbb{V}_q, \quad (9)$$

where the quantum numbers can only be the trivial and the non-trivial irreps, $q = 0$ and $q = 1$, respectively. The physical index of the coarse-grained PEPS tensor is then given by

$$\mathbb{V}_p = (0_1 \oplus 1_1)^{\otimes 6} = (0_{32} \oplus 1_{32}). \quad (10)$$

However, then implementing the \mathbb{Z}_2 symmetry in the usual way, we are facing two problems: (i) the spiral PEPS ansatz can no longer be used because the local unitary transformations are non-symmetric, and (ii) for the potential \mathbb{Z}_2 QSL ground state, the symmetry is expected to emerge only at the virtual indices of the PEPS tensor without acting globally as described above. The first point can be mitigated by enlarging the unit cell back to 18 sites, albeit at a significantly higher computational cost, that is prohibitively large to reach $\chi_B = 8$

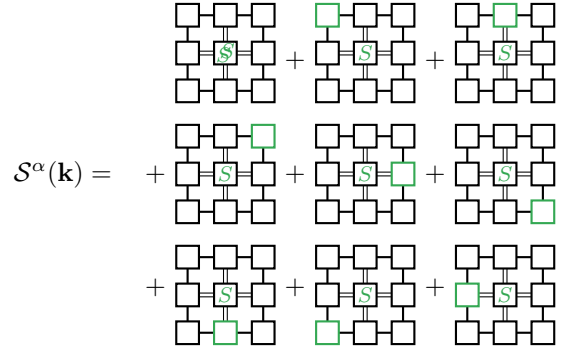
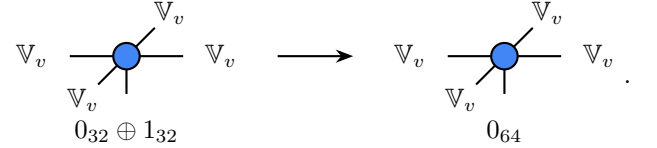


FIG. 6. Calculation of one component of the static spin structure factor in Eq. (11). Each green tensor contains all phases and the action of the spin operators arising from the respective semi-infinite part of the square lattice. In the first diagram, both spin operators act on the same site, while in the remaining ones there is only one local operator.

as for the spiral ansatz. However, we can eliminate both obstacles by a simple change in the network. Instead of representing the physical index in a symmetry-preserving form, we represent the physical Hilbert space according to



Since we only use the trivial irrep $q = 0$, the unitary spiral transformations can again be done in its degenerate space, and the \mathbb{Z}_2 symmetry acts entirely on the virtual indices.

Calculation of structure factors

In this section we will outline the calculation of PEPS structure factors, based on a modified CTMRG summation scheme [71, 72]. While this scheme is approximate and more refined schemes have been proposed [73, 74], the short correlation lengths and large coarse-grained six-site basis justify its use. We first illustrate the procedure for a regular square lattice, and after that highlight the modifications for non-Bravais lattices such as the MLL. Exploiting translational invariance of the PEPS ansatz, the square lattice structure factor is given by

$$\begin{aligned} \mathcal{S}(\mathbf{k}) &= \sum_{\alpha} \mathcal{S}^{\alpha}(\mathbf{k}) \\ &= \sum_{\alpha} \sum_{x,y} e^{i(k_x x + k_y y)} \langle \Psi | S_{(x,y)}^{\alpha} \cdot S_{(0,0)}^{\alpha} | \Psi \rangle, \end{aligned} \quad (11)$$

where α runs over all spin components $[x, y, z]$. Each part $\mathcal{S}^{\alpha}(\mathbf{k})$ can be computed by summing up different tensor network diagrams, as shown in Fig. 6. In each diagram, the

phases $\exp(i(k_x x + k_y y))$ and the action of the spin operators S^α at position (x, y) are contained in modified CTMRG environment tensors, shown in green. They collect the individual contributions of the structure factor arising from the respective semi-infinite part of the square lattice. The remaining black environment tensors are those for the norm of the infinite PEPS. The local tensor contains either the effect of both spin operators at the same position $(0, 0)$, or a single spin operator at this position. The phases and spin operators for each lattice site (x, y) can be accounted for in a modified CTMRG absorption routine. To this end, each CTMRG run computes two sets of environment tensors, one for the norm of the quantum state and one that contains the structure factor components. For the directional CTMRG we make the (somewhat arbitrary) choice, that a bottom absorption is along the lattice vector \mathbf{a}_1 and a right absorption is along the lattice vector \mathbf{a}_2 . Consequently, a top absorption is performed along $-\mathbf{a}_1$ and a left absorption along $-\mathbf{a}_2$. Focusing on a left absorption move, the regular edge tensor T is updated by

$$T' \square = \text{Diagram showing a square tensor with a vertical line on the left and a horizontal line on the right, updated by a diagram showing a square tensor with a vertical line on the left and a horizontal line on the right, with a green square inside and a black square to its right, all within a larger square frame with diagonal lines.$$

While absorbing a PEPS tensor and its conjugate, projectors are required to reduce the bond dimension back to χ_E by restricting to the most important subspace. The corner tensors C are updated in a similar fashion, absorbing an edge tensor and using truncation projectors, i.e.,

$$C' \square = \text{Diagram showing a square tensor with a vertical line on the left and a horizontal line on the right, updated by a diagram showing a square tensor with a vertical line on the left and a horizontal line on the right, with a green square inside and a black square to its right, all within a larger square frame with diagonal lines.$$

For the edge tensor T_p containing the phases and spin operators, the absorption is given by

$$T'_p \square = \left(\text{Diagram 1} + \text{Diagram 2} \right) \cdot e^{-ik a_2}.$$

In the first part a regular PEPS tensor is absorbed, thereby shifting all operators already contained in T_p , one lattice site to the left. In the second part, a new spin operator S^α is absorbed into the left boundary tensor T . When weighted with the corresponding phase, the tensor T_p will converge to a collection of terms

$$T_p \sim \dots + e^{-i2k_y} S^\alpha_{(-2,0)} + e^{-ik_y} S^\alpha_{(-1,0)}, \quad (12)$$

which generates all structure factor contributions for the semi-infinite row left of site $(0, 0)$. The corner tensors containing phases and operators is updated by

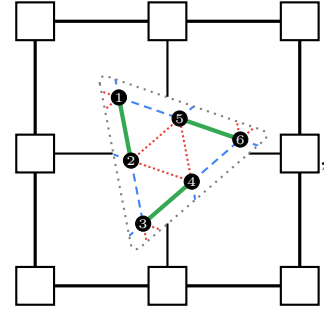
$$C'_p \square = \left(\text{Diagram 1} + \text{Diagram 2} \right) \cdot e^{-ik a_2}.$$

Since every corner partakes in two perpendicular absorption steps, it collects all structure factor contributions in one semi-infinite corner of the network. Let us note, that there are several subtleties in the CTMRG routine, especially when used for a non-trivial PEPS unit cell [44]. For the environment tensors containing phase factors and spin operators, it is also crucial to normalize them with respect to the environment tensors for the norm of the quantum state, so that the diagrams in Fig. 6 are not skewed.

The extension to non-Bravais lattices such as the MLL is now rather straightforward. Due to the non-trivial basis, the structure factor in Eq. (11) needs two additional sums over the basis sites and relative phase factors between them. It is given by

$$S(\mathbf{k}) = \sum_{i,j} \sum_{m,n} e^{i\mathbf{k} \cdot (\mathbf{R}_i - \mathbf{R}_j)} e^{i\mathbf{k} \cdot (\mathbf{b}_m - \mathbf{b}_n)} \times \langle \mathbf{S}(\mathbf{R}_i + \mathbf{b}_m) \cdot \mathbf{S}(\mathbf{R}_j + \mathbf{b}_n) \rangle. \quad (13)$$

For the specific case of the MLL with a basis of $N_B = 6$ sites, the first TN diagram in Fig. 6 now contains local correlations within the cluster



with a total of $N_B \cdot N_B$ different spin-spin correlations, including phases $\exp(i\mathbf{k} \cdot (\mathbf{b}_m - \mathbf{b}_n))$. The remaining diagrams are also affected by one of the loops over the basis sites with phases $\exp(-i\mathbf{k} \cdot \mathbf{b}_n)$. The second one however appears in the update of the T_p tensors, which now have to include *relative* phases and the action of the spin operator on all basis sites. For a generic non-Bravais lattice, that can be treated with a CTMRG routine on a square lattice, the generalized absorption is given by

$$T'_p \square = \left(\text{Diagram 1} + \sum_{m=1}^{N_B} e^{+i\mathbf{k} \cdot \mathbf{b}_m} \text{Diagram 2} \right) \cdot e^{-ik a_2}. \quad (14)$$

The spin operator S^α needs to be applied to the m -th basis site of the local PEPS tensor in the summation. The update of the corner tensors C_p remains unchanged.

Structure factor analysis

We present the equal-time spin structure factors for the isotropic ruby lattice and MLL in Fig. 7 which show broad similarities, being peaked at the K -points of the extended Brillouin zone. To highlight the differences in the structure

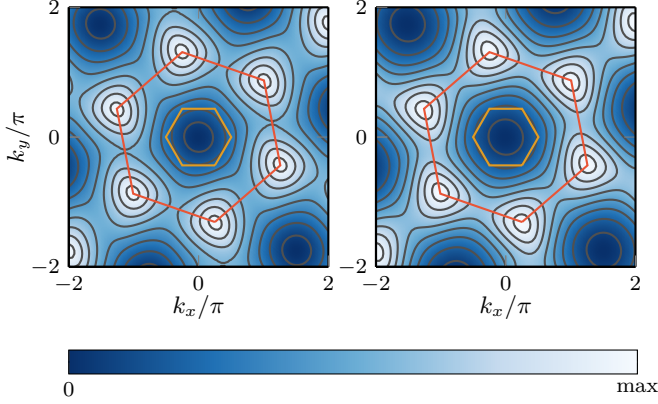


FIG. 7. Equal-time structure factors $\mathcal{S}(\mathbf{k})$ for the ruby lattice at $J_g = 0$ (left) and MLL at $J_g = 1$ (right). The first and extended Brillouin zones are indicated in orange and red, respectively.

factors, we present a plot of the path in the extended Brillouin zone in Fig. 8, traversing from $\Gamma \mapsto M' \mapsto K' \mapsto \Gamma$. Both curves follow a similar profile, with only moderate differences in slope and absolute value. This is intriguing given the fact that the ground states of the isotropic ruby and maple-leaf lattices exhibit profoundly different characteristics (i.e., gapless vs. gapped).

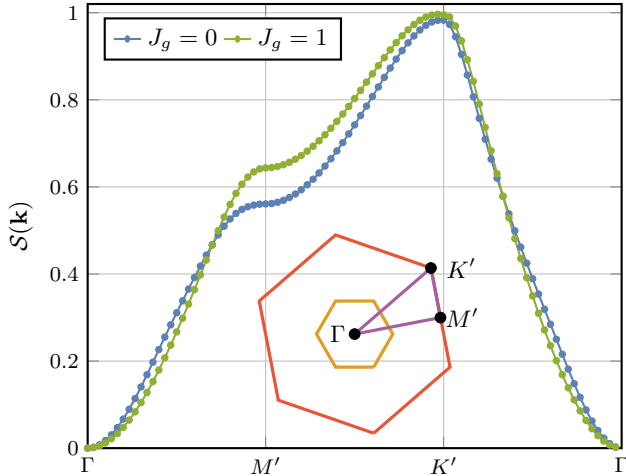


FIG. 8. Structure factor calculated along the path inside the extended Brillouin zone from the Γ point to M' , K' and back to the Γ point (purple path in the inset). In orange the Brillouin zone and in red the extended Brillouin zone are indicated.

Finite bond dimension extrapolation

Coupling J_g	$J_g = 0$	$J_g = 1$
Estimate	-0.563781	-0.530359
Lowest variational energy	-0.561402	-0.528588
Linear fit	-0.565328	-0.533659

TABLE II. Comparison of energy estimate from actual fits as described in the main text, lowest variational energies, and linear fit results for the ruby and MLL.

The fixed bulk bond dimension χ_B of the tensor network imposes an effective length scale on the quantum states. It is given by the correlation length ξ , which can be conveniently computed from the infinite PEPS transfer matrix and is typically used in heuristic extrapolations of both the ground state energy and the magnetization [58–60]. In the infinite PEPS for the MLL, the correlation length is calculated in the coarse-grained picture. In order to transfer it to the original lattice, it must be scaled by a factor of $\sqrt{7}$. Unfortunately, it turned out to be unsuitable for extrapolation in our study. We therefore have to resort to less sophisticated methods based on direct inverse bond dimension analysis. Here, we will present a small subset of the performed extrapolations to visualize the procedure. In the gapless regime we use an algebraic fit [8, 61] in the form of $E_0(\chi_B) = E_0 + a\chi_B^{-\alpha}$ to extract the infinite bond dimension limit. This is visualized in Fig. 9, for a fit of the five largest data points. Once the free exponent α reaches $\alpha = 2$, we transition to using a fixed polynomial fit in the form of $E_0(\chi_B) = E_0 + a \cdot \chi_B^{-2}$ for the gapped phases. The transition in the fits occurs at around $J_g = 0.59$, which deviates from the estimation of the transition from the susceptibility to an external magnetic field. However, this analysis was performed at

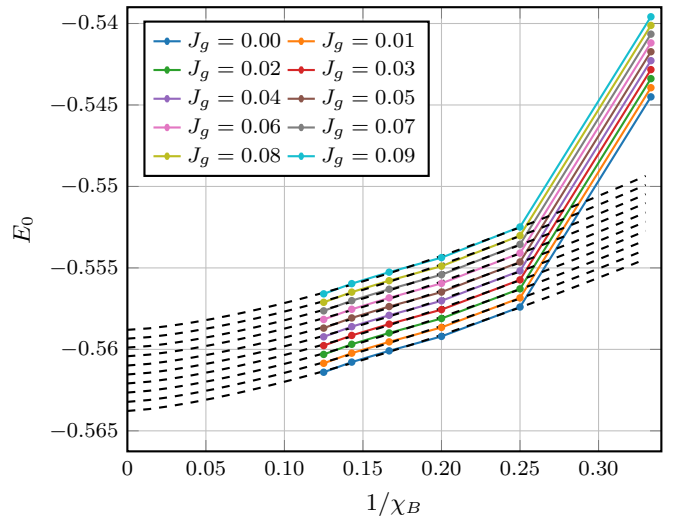


FIG. 9. Convergence of the ground state energy and infinite bond dimension extrapolation in the gapless region of the phase diagram for small J_g .

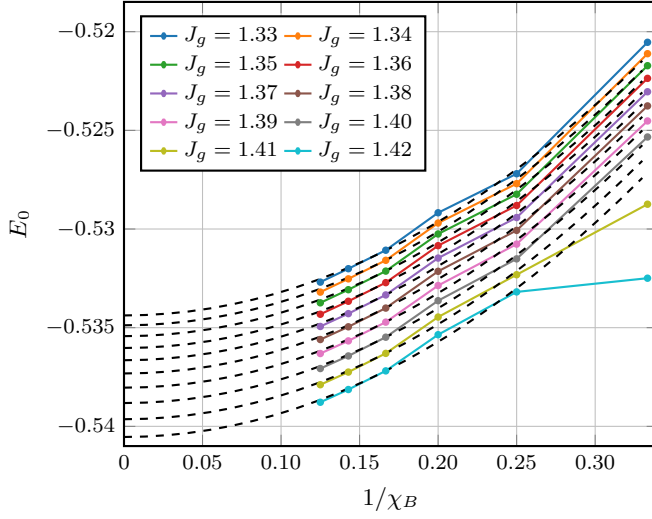


FIG. 10. Convergence of the ground state energy and infinite bond dimension extrapolation in the magnetically ordered region of the phase diagram.

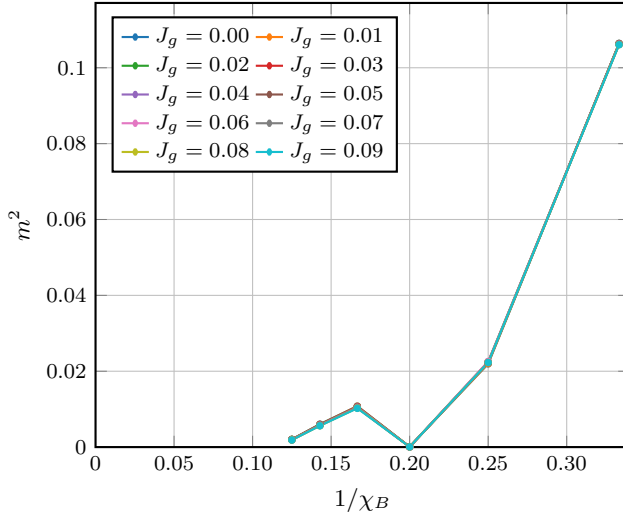


FIG. 11. Convergence of the staggered magnetization in the gapless region of the phase diagram for small J_g . The non-magnetic states are clearly visible.

a fixed bond dimension of $\chi_B = 5$, while the infinite bond dimension extrapolation takes values $\chi_B = \{4, 5, 6, 7, 8\}$ into account. With a possible shift of the actual transition with increasing χ_B , the agreement is acceptable. In Fig. 10 we demonstrate the extrapolation of the energy for the magnet-

ically ordered region. Here we focus on the interval of J_g , in which the infinite bond dimension extrapolation actually yields a finite value (c.f. Fig. 12). It is noticeable that the energy for small J_g shows a smoother convergence with the bond dimension χ_B than, for example, in the magnetically ordered phase. This is due to the different levels of frustration in the model. For high frustration, it is significantly more difficult for the variational PEPS optimization to reach the ground state and overcome local energy minima.

In order to estimate an error for the ground state energy we perform the following analysis. A linear fit of the data points should provide a meaningful lower bound E_l [62]. The largest data point at $\chi_B = 8$ provides the lowest variational upper bound E_u to the energy. As an error to the extrapolated value from the fit we then use $\Delta E = (E_u - E_l)/2$. For the ruby and maple-leaf lattice, this results in the values reported in Table II.

Next, we present the convergence and extrapolation for the staggered magnetization m^2 . Focusing on small J_g in the gapless phase, i.e., at the ruby lattice and above, its behaviour indicates a vanishing order parameter, even with the untypical non-monotonic convergence of the iPEPS simulations, as shown in Fig. 11. This behaviour is found consistently throughout the large non-magnetic phase, and a proper fit is not even required to extract its limit. Finally, in the region of magnetic order we use a first-order polynomial fit of the five largest data points to extract the infinite χ_B limit.

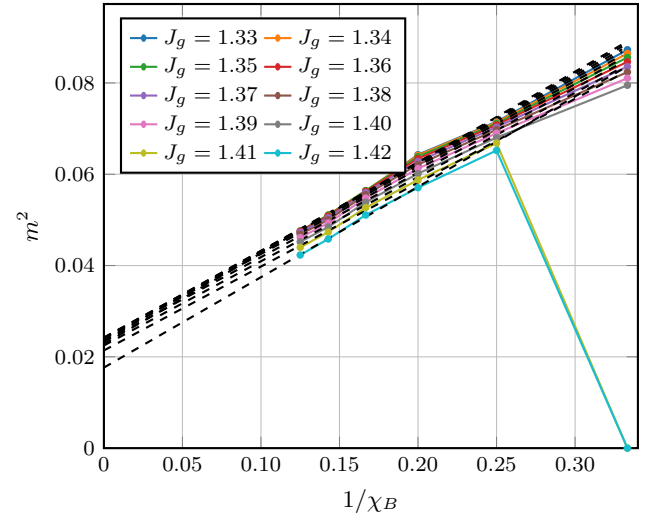


FIG. 12. Convergence of the staggered magnetization and infinite bond dimension extrapolation in the magnetically ordered region of the phase diagram.

Ground state energy data

This section presents the numerical data for the per-spin ground state energy E_0 for the different PEPS bond dimensions χ_B (labeled D in the table) as a function of the interaction strength J_g , as well as their extrapolation.

J_g	D3	D4	D5	D6	D7	D8	Extrapolation
0	-0.544503	-0.557401	-0.559204	-0.560091	-0.560781	-0.561402	-0.563781
0.01	-0.543942	-0.556841	-0.558653	-0.55954	-0.560232	-0.560854	-0.563216
0.02	-0.543384	-0.556285	-0.558105	-0.558993	-0.559686	-0.560309	-0.56265
0.03	-0.542831	-0.555732	-0.55756	-0.558449	-0.559144	-0.559767	-0.562093
0.04	-0.542281	-0.555183	-0.55702	-0.557908	-0.558605	-0.559229	-0.561537
0.05	-0.541734	-0.554637	-0.556483	-0.557371	-0.55807	-0.558694	-0.560984
0.06	-0.541192	-0.554094	-0.555949	-0.556839	-0.557539	-0.558163	-0.560432
0.07	-0.540653	-0.553555	-0.555419	-0.556309	-0.55701	-0.557636	-0.559886
0.08	-0.540118	-0.553019	-0.554892	-0.555784	-0.556487	-0.557112	-0.559345
0.09	-0.539587	-0.552487	-0.554369	-0.555262	-0.555965	-0.556592	-0.558806
0.1	-0.53906	-0.551958	-0.55385	-0.554743	-0.555448	-0.556076	-0.558273
0.11	-0.538537	-0.551433	-0.553335	-0.554227	-0.554935	-0.555563	-0.557744
0.12	-0.538017	-0.550912	-0.552823	-0.553716	-0.554426	-0.555055	-0.557217
0.13	-0.537502	-0.550394	-0.552315	-0.553209	-0.553919	-0.554549	-0.556691
0.14	-0.53699	-0.549879	-0.55181	-0.552705	-0.553416	-0.554048	-0.556177
0.15	-0.536483	-0.549368	-0.551309	-0.552205	-0.552919	-0.553551	-0.555661
0.16	-0.535979	-0.548861	-0.550812	-0.551709	-0.552424	-0.553057	-0.55515
0.17	-0.53548	-0.548358	-0.550319	-0.551215	-0.551934	-0.552567	-0.554645
0.18	-0.534984	-0.547858	-0.549829	-0.550727	-0.551447	-0.552081	-0.554142
0.19	-0.534493	-0.547362	-0.549344	-0.550243	-0.550964	-0.551599	-0.553644
0.2	-0.534006	-0.546869	-0.548862	-0.549761	-0.550484	-0.55112	-0.553149
0.21	-0.533523	-0.54638	-0.548384	-0.549285	-0.550009	-0.550646	-0.552658
0.22	-0.533044	-0.545896	-0.54791	-0.548812	-0.549539	-0.550176	-0.552173
0.23	-0.53257	-0.545414	-0.54744	-0.548343	-0.549072	-0.54971	-0.551692
0.24	-0.5321	-0.544937	-0.546974	-0.547878	-0.548609	-0.549248	-0.551214
0.25	-0.531634	-0.544464	-0.546511	-0.547416	-0.548149	-0.548789	-0.55074
0.26	-0.531172	-0.543994	-0.546054	-0.546959	-0.547694	-0.548334	-0.550265
0.27	-0.530715	-0.543528	-0.545599	-0.546506	-0.547244	-0.547885	-0.549806
0.28	-0.530262	-0.543066	-0.545149	-0.546057	-0.546797	-0.547439	-0.549346
0.29	-0.529814	-0.542608	-0.544702	-0.545612	-0.546354	-0.546997	-0.548891
0.3	-0.52937	-0.542154	-0.54426	-0.545172	-0.545915	-0.54665	-0.548438
0.31	-0.528931	-0.541704	-0.543823	-0.544735	-0.54548	-0.546127	-0.547987
0.32	-0.528496	-0.541258	-0.543389	-0.544303	-0.545051	-0.545696	-0.547542
0.33	-0.528066	-0.540816	-0.54296	-0.543874	-0.544625	-0.545271	-0.547098
0.34	-0.52764	-0.540378	-0.542534	-0.543451	-0.544204	-0.54485	-0.546669
0.35	-0.527219	-0.539944	-0.542112	-0.543031	-0.543786	-0.544435	-0.546245
0.36	-0.526803	-0.539515	-0.541697	-0.542615	-0.543373	-0.544023	-0.545813
0.37	-0.526392	-0.539089	-0.541283	-0.542205	-0.542965	-0.543614	-0.545393
0.38	-0.525985	-0.538667	-0.540875	-0.541798	-0.542561	-0.543214	-0.544983
0.39	-0.525583	-0.53825	-0.54047	-0.541396	-0.542161	-0.542814	-0.54457
0.4	-0.525186	-0.537837	-0.540071	-0.540999	-0.541766	-0.542419	-0.544158
0.41	-0.524794	-0.537428	-0.539675	-0.540608	-0.541374	-0.542031	-0.543759
0.42	-0.524407	-0.537023	-0.539285	-0.54022	-0.540989	-0.541646	-0.543357
0.43	-0.524024	-0.536623	-0.538898	-0.539836	-0.540607	-0.541265	-0.542965
0.44	-0.523647	-0.536227	-0.538516	-0.539457	-0.540229	-0.54089	-0.542578
0.45	-0.523275	-0.535835	-0.538139	-0.539082	-0.539857	-0.540517	-0.542191
0.46	-0.522908	-0.535448	-0.537766	-0.538712	-0.539489	-0.540152	-0.541816
0.47	-0.522546	-0.535065	-0.537399	-0.538346	-0.539126	-0.539789	-0.541436
0.48	-0.52219	-0.534687	-0.537034	-0.537988	-0.538768	-0.539433	-0.541071
0.49	-0.521838	-0.534313	-0.536675	-0.537632	-0.538414	-0.539081	-0.540704
0.5	-0.521492	-0.533943	-0.536321	-0.537279	-0.538065	-0.538734	-0.540355
0.51	-0.521151	-0.533578	-0.535971	-0.536933	-0.537721	-0.538392	-0.54
0.52	-0.520816	-0.533218	-0.535626	-0.536592	-0.537381	-0.538054	-0.539651
0.53	-0.520486	-0.532862	-0.535287	-0.536255	-0.537047	-0.537721	-0.539303
0.54	-0.520162	-0.532511	-0.534951	-0.535923	-0.536718	-0.537393	-0.53897
0.55	-0.519843	-0.532164	-0.534621	-0.535596	-0.536394	-0.537071	-0.538638
0.56	-0.51953	-0.531822	-0.534296	-0.535274	-0.536074	-0.536753	-0.538309
0.57	-0.519222	-0.531485	-0.533975	-0.534957	-0.53576	-0.536441	-0.537986
0.58	-0.518921	-0.531153	-0.533659	-0.534644	-0.53545	-0.536134	-0.537674
0.59	-0.518625	-0.530825	-0.533349	-0.534338	-0.535146	-0.535831	-0.53736
0.6	-0.518334	-0.530503	-0.533042	-0.534035	-0.534847	-0.535534	-0.536969
0.61	-0.51805	-0.530185	-0.532741	-0.533738	-0.534553	-0.535243	-0.536658
0.62	-0.517772	-0.529872	-0.532447	-0.533447	-0.534265	-0.534955	-0.53634
0.63	-0.5175	-0.529564	-0.532155	-0.533161	-0.533981	-0.534671	-0.536028
0.64	-0.517234	-0.529261	-0.53187	-0.532879	-0.533703	-0.534399	-0.535716
0.65	-0.516974	-0.528963	-0.531589	-0.532603	-0.53343	-0.53413	-0.535404
0.66	-0.51672	-0.528671	-0.531316	-0.532332	-0.533163	-0.533863	-0.535092
0.67	-0.516472	-0.528383	-0.531045	-0.532067	-0.532901	-0.533607	-0.53478
0.68	-0.516231	-0.528101	-0.530781	-0.531807	-0.532645	-0.533352	-0.53447
0.69	-0.515997	-0.527824	-0.530524	-0.531553	-0.532394	-0.533104	-0.53416
0.7	-0.515769	-0.527552	-0.53027	-0.531304	-0.532149	-0.532861	-0.53385

Jg	D3	D4	D5	D6	D7	D8	Extrapolation
0.71	-0.515547	-0.527285	-0.53002	-0.53106	-0.53191	-0.532625	-0.534128
0.72	-0.515332	-0.527024	-0.529779	-0.530823	-0.531676	-0.532394	-0.533903
0.73	-0.515124	-0.526768	-0.529542	-0.530592	-0.531447	-0.532168	-0.533683
0.74	-0.514923	-0.526518	-0.529312	-0.530366	-0.531226	-0.531949	-0.533471
0.75	-0.514729	-0.526274	-0.529086	-0.530145	-0.531009	-0.531736	-0.533265
0.76	-0.514541	-0.526035	-0.528867	-0.52993	-0.530799	-0.531528	-0.533064
0.77	-0.514361	-0.525801	-0.528653	-0.529722	-0.530595	-0.531327	-0.53287
0.78	-0.514188	-0.525574	-0.528444	-0.529519	-0.530397	-0.531131	-0.532684
0.79	-0.514022	-0.525352	-0.528242	-0.529321	-0.530203	-0.530942	-0.532502
0.8	-0.513864	-0.525137	-0.528045	-0.529131	-0.530018	-0.530759	-0.532328
0.81	-0.513713	-0.524927	-0.527855	-0.528946	-0.529836	-0.530583	-0.532159
0.82	-0.51357	-0.524723	-0.527665	-0.528768	-0.529663	-0.530413	-0.532003
0.83	-0.513434	-0.524525	-0.527493	-0.528596	-0.529495	-0.530249	-0.531841
0.84	-0.513307	-0.524334	-0.527321	-0.52843	-0.529335	-0.530092	-0.531693
0.85	-0.513187	-0.524149	-0.527153	-0.52827	-0.529179	-0.529994	-0.531608
0.86	-0.513075	-0.52397	-0.526996	-0.528117	-0.529033	-0.529797	-0.531417
0.87	-0.512971	-0.523798	-0.526843	-0.52797	-0.528891	-0.529659	-0.531287
0.88	-0.512876	-0.523633	-0.526696	-0.52783	-0.528756	-0.529583	-0.531223
0.89	-0.512789	-0.523474	-0.526555	-0.527696	-0.528628	-0.529405	-0.531053
0.9	-0.51271	-0.523322	-0.526422	-0.527569	-0.528506	-0.529288	-0.530945
0.91	-0.51264	-0.523177	-0.526294	-0.527449	-0.528392	-0.529225	-0.530895
0.92	-0.512579	-0.523039	-0.526175	-0.527336	-0.528285	-0.529075	-0.530752
0.93	-0.512527	-0.522909	-0.526061	-0.527229	-0.528183	-0.529042	-0.530732
0.94	-0.512484	-0.522785	-0.525952	-0.527129	-0.528091	-0.528914	-0.530615
0.95	-0.512451	-0.52267	-0.525854	-0.527037	-0.528005	-0.528834	-0.530545
0.96	-0.512426	-0.522562	-0.525761	-0.526952	-0.527926	-0.528802	-0.530526
0.97	-0.512412	-0.522462	-0.525676	-0.526874	-0.527855	-0.528737	-0.530472
0.98	-0.512407	-0.52237	-0.525596	-0.526804	-0.527791	-0.528679	-0.530427
0.99	-0.512412	-0.522287	-0.525526	-0.52674	-0.527733	-0.52863	-0.530388
1	-0.512427	-0.522212	-0.525462	-0.526684	-0.527686	-0.528588	-0.530359
1.01	-0.512452	-0.522146	-0.525405	-0.526637	-0.527645	-0.528513	-0.530295
1.02	-0.512488	-0.522089	-0.525356	-0.526596	-0.527612	-0.528489	-0.530284
1.03	-0.512535	-0.522041	-0.525314	-0.526564	-0.527587	-0.52848	-0.530289
1.04	-0.512592	-0.522003	-0.525281	-0.526539	-0.527569	-0.528496	-0.530318
1.05	-0.512661	-0.521975	-0.525256	-0.526522	-0.527561	-0.528501	-0.530337
1.06	-0.512741	-0.521957	-0.525237	-0.526515	-0.527561	-0.52851	-0.530361
1.07	-0.512833	-0.52195	-0.525228	-0.526514	-0.527568	-0.528526	-0.53039
1.08	-0.512937	-0.521954	-0.525226	-0.526523	-0.527586	-0.528553	-0.530432
1.09	-0.513053	-0.521969	-0.525233	-0.526539	-0.527611	-0.528587	-0.530481
1.1	-0.513182	-0.521996	-0.525248	-0.526565	-0.527645	-0.528629	-0.530538
1.11	-0.513323	-0.522036	-0.525272	-0.526599	-0.527688	-0.528683	-0.530607
1.12	-0.513477	-0.522088	-0.525302	-0.526643	-0.527741	-0.528744	-0.530687
1.13	-0.513645	-0.522153	-0.525345	-0.526695	-0.527802	-0.528844	-0.530802
1.14	-0.513826	-0.522233	-0.525395	-0.526757	-0.527873	-0.528901	-0.530876
1.15	-0.514022	-0.522326	-0.525454	-0.526828	-0.527954	-0.528988	-0.530979
1.16	-0.514232	-0.522434	-0.525523	-0.526908	-0.528045	-0.529078	-0.531087
1.17	-0.514457	-0.522558	-0.5256	-0.526999	-0.528145	-0.5292	-0.531227
1.18	-0.514697	-0.522697	-0.525688	-0.527099	-0.528256	-0.529325	-0.531371
1.19	-0.514953	-0.522854	-0.525785	-0.527209	-0.528377	-0.529459	-0.531524
1.2	-0.515225	-0.523027	-0.525892	-0.52733	-0.528509	-0.529601	-0.531686
1.21	-0.515514	-0.523218	-0.526009	-0.527462	-0.528651	-0.529757	-0.531862
1.22	-0.515821	-0.523428	-0.526137	-0.527604	-0.528805	-0.529925	-0.532051
1.23	-0.516145	-0.523657	-0.526275	-0.527757	-0.528969	-0.530104	-0.532251
1.24	-0.516488	-0.523907	-0.526424	-0.527922	-0.529145	-0.530295	-0.532464
1.25	-0.516849	-0.524177	-0.526584	-0.528123	-0.529333	-0.530497	-0.532691
1.26	-0.517231	-0.524468	-0.526755	-0.528387	-0.529533	-0.530713	-0.532939
1.27	-0.517633	-0.524783	-0.526938	-0.528681	-0.529746	-0.530941	-0.533201
1.28	-0.518058	-0.52512	-0.527133	-0.529004	-0.52997	-0.531182	-0.533478
1.29	-0.518504	-0.525482	-0.527402	-0.529357	-0.530278	-0.531436	-0.533767
1.3	-0.518974	-0.52587	-0.527802	-0.52974	-0.530664	-0.531705	-0.534019
1.31	-0.519469	-0.526284	-0.52823	-0.530153	-0.531081	-0.531989	-0.534287
1.32	-0.519989	-0.526726	-0.528688	-0.530598	-0.53153	-0.532286	-0.534571
1.33	-0.520538	-0.527198	-0.529176	-0.531075	-0.532011	-0.532691	-0.534966
1.34	-0.521115	-0.527701	-0.529697	-0.531587	-0.532525	-0.533197	-0.535466
1.35	-0.521723	-0.528237	-0.530252	-0.532133	-0.533075	-0.53374	-0.536004
1.36	-0.522365	-0.528809	-0.530843	-0.532717	-0.533662	-0.534319	-0.536579
1.37	-0.523044	-0.529419	-0.531473	-0.533341	-0.534288	-0.534939	-0.537194
1.38	-0.523762	-0.53007	-0.532143	-0.534007	-0.534955	-0.535601	-0.537854
1.39	-0.524524	-0.530766	-0.532864	-0.534719	-0.535669	-0.53631	-0.538557
1.4	-0.525336	-0.531513	-0.533632	-0.535482	-0.536433	-0.537071	-0.539314
1.41	-0.528743	-0.532317	-0.534461	-0.536302	-0.53725	-0.537891	-0.540125
1.42	-0.532493	-0.533187	-0.535356	-0.537189	-0.538135	-0.538779	-0.541005
1.43	-0.536243	-0.536247	-0.536333	-0.538158	-0.539097	-0.539758	-0.541972
1.44	-0.53999	-0.539996	-0.539996	-0.539238	-0.54017	-0.54086	-0.542915
1.45	-0.543714	-0.543746	-0.543746	-0.543719	-0.543744	-0.543899	-0.54375
1.46	-0.547477	-0.54749	-0.547495	-0.547465	-0.547494	-0.548549	-0.5475
1.47	-0.551192	-0.551244	-0.551245	-0.55121	-0.551243	-0.550874	-0.55125
1.48	-0.554989	-0.554994	-0.554995	-0.554956	-0.554993	-0.555522	-0.555
1.49	-0.558723	-0.558747	-0.558745	-0.558702	-0.558743	-0.560171	-0.55875
1.5	-0.562447	-0.562491	-0.562495	-0.562447	-0.562493	-0.562499	-0.5625

Ground state magnetization data

This section presents the numerical data for the per-spin staggered magnetization m^2 for the different PEPS bond dimensions χ_B (labelled D in the table) as a function of the interaction strength J_g , as well as their extrapolation.

J_g	D3	D4	D5	D6	D7	D8	Extrapolation
0	0.106440503	0.021939993	0.000089672	0.010801723	0.006050351	0.002054055	0
0.01	0.106399239	0.021996915	0.000090278	0.010782647	0.005998186	0.002034264	0
0.02	0.106361472	0.022450368	0.000086382	0.010652785	0.00595284	0.002012661	0
0.03	0.106317039	0.02230287	0.000059129	0.010631049	0.005885748	0.001986792	0
0.04	0.106273868	0.022515683	0.00005969	0.010545367	0.005831977	0.001963741	0
0.05	0.106240387	0.022361461	0.000062576	0.01038765	0.005769039	0.00194409	0
0.06	0.106187001	0.022577181	0.000066698	0.010419133	0.005737676	0.001916989	0
0.07	0.106146169	0.022271043	0.000064327	0.010407841	0.005686132	0.001893987	0
0.08	0.106101961	0.022331532	0.000061462	0.010286117	0.005630508	0.00187706	0
0.09	0.106059383	0.0223023	0.000058648	0.010218599	0.005616107	0.001861126	0
0.1	0.106014171	0.022434137	0.000050799	0.010102037	0.005533102	0.001852575	0
0.11	0.105969063	0.022386621	0.000056865	0.009972425	0.005458352	0.001844586	0
0.12	0.105923465	0.022440309	0.000054935	0.00992173	0.005413313	0.001829448	0
0.13	0.1058756	0.022661607	0.000050489	0.00983061	0.005384922	0.001699615	0
0.14	0.105830675	0.022800543	0.000043091	0.009725069	0.005330108	0.001789203	0
0.15	0.105784121	0.022662705	0.000042575	0.009695641	0.005246517	0.001771236	0
0.16	0.105740045	0.022895267	0.000043118	0.009603324	0.005180772	0.001750697	0
0.17	0.105691748	0.023105244	0.000034009	0.00941053	0.005163724	0.001727255	0
0.18	0.105642861	0.022790221	0.000034198	0.009399581	0.005127826	0.001697659	0
0.19	0.105596943	0.022875218	0.000040474	0.009281408	0.00504063	0.001676091	0
0.2	0.105549805	0.02313112	0.000039053	0.009261101	0.004983046	0.001660225	0
0.21	0.105499629	0.023248392	0.000032038	0.009230335	0.004999269	0.001635599	0
0.22	0.10545408	0.023049933	0.000033083	0.009079067	0.004883035	0.001618434	0
0.23	0.10540055	0.023188086	0.000032512	0.009052515	0.004837956	0.001590741	0
0.24	0.105353184	0.023219593	0.00003198	0.008936721	0.004782865	0.001528117	0
0.25	0.105302519	0.02356932	0.000029967	0.008934653	0.004735135	0.001553062	0
0.26	0.105252376	0.023448062	0.000000062	0.008846424	0.004740439	0.001548521	0
0.27	0.105201611	0.023516815	0.000028369	0.008785548	0.004641436	0.001471724	0
0.28	0.105153794	0.023522782	0.000024082	0.008635177	0.00458955	0.001448804	0
0.29	0.105096669	0.023468242	0.000027746	0.008537981	0.004540449	0.001406824	0
0.3	0.105044946	0.023801117	0.000027492	0.008460074	0.004536447	0.001404044	0
0.31	0.104994878	0.023809255	0.000000766	0.008359139	0.004438827	0.001356207	0
0.32	0.104941321	0.02409017	0.000022151	0.00829159	0.004424588	0.001446461	0
0.33	0.104889433	0.023929748	0.000001172	0.008176429	0.00440882	0.001439888	0
0.34	0.104833892	0.023969579	0.00002632	0.008079019	0.004322246	0.001409326	0
0.35	0.104780865	0.023977256	0.000026997	0.007987998	0.004279776	0.001297917	0
0.36	0.104727591	0.024122247	0.000000954	0.007891584	0.004234986	0.00131104	0
0.37	0.104680204	0.024352126	0.000024887	0.007765747	0.004216686	0.001343114	0
0.38	0.104611095	0.024380447	0.000002634	0.007640901	0.004131775	0.001129611	0
0.39	0.104554227	0.024593606	0.000024561	0.007462442	0.004122806	0.001202926	0
0.4	0.104503253	0.024680711	0.000025611	0.007131674	0.004083324	0.001234701	0
0.41	0.104445913	0.025100075	0.00002443	0.006929093	0.004043847	0.00103609	0
0.42	0.104387839	0.025015889	0.000011476	0.006884952	0.003993299	0.001038396	0
0.43	0.104328731	0.025005403	0.000025727	0.006833315	0.003932177	0.001040322	0
0.44	0.104269685	0.025131442	0.000024717	0.00682199	0.003886891	0.000966856	0
0.45	0.104210411	0.025084344	0.000026273	0.006762012	0.003852692	0.001045374	0
0.46	0.104149089	0.025267562	0.000025282	0.006681907	0.003780716	0.000936952	0
0.47	0.104089582	0.02557431	0.000000035	0.006701198	0.003721422	0.000956444	0
0.48	0.104028891	0.025769309	0.000025665	0.006523368	0.003686477	0.000812043	0
0.49	0.10396494	0.025783186	0.000016589	0.00644643	0.003676033	0.000821655	0
0.5	0.103904622	0.026029918	0.000025962	0.006531611	0.003614712	0.00063693	0
0.51	0.103839664	0.025885259	0.000042263	0.006320757	0.003571751	0.000601969	0
0.52	0.103775881	0.026370296	0.000022987	0.006278647	0.003539314	0.000610954	0
0.53	0.103715171	0.026561791	0.000000256	0.006257887	0.003457302	0.00057557	0
0.54	0.103646195	0.026506355	0.000028304	0.006184099	0.003457036	0.000533334	0
0.55	0.103576684	0.026751297	0.000004875	0.0061823	0.003421145	0.00043775	0
0.56	0.103516999	0.026853847	0.000000039	0.006093405	0.003383478	0.000431034	0
0.57	0.103450426	0.02693659	0.000000069	0.006049406	0.003332948	0.000425185	0
0.58	0.103379174	0.027122566	0.000018385	0.006009366	0.003265024	0.000360203	0
0.59	0.103308516	0.027695403	0.000000456	0.006041826	0.003255298	0.000353394	0
0.6	0.10324306	0.027560522	0.000012856	0.005919955	0.003208761	0.000338616	0
0.61	0.103169548	0.027675101	0.000001569	0.005857532	0.003138958	0.000336543	0
0.62	0.103105581	0.028161298	0.000000836	0.00584774	0.003126299	0.000335087	0
0.63	0.103031364	0.028106124	0.000002178	0.005856395	0.003092932	0.000249296	0
0.64	0.102952464	0.028484278	0.000001088	0.005751509	0.003048428	0.00024738	0
0.65	0.102880352	0.028714189	0.000023745	0.005712841	0.00297688	0.000164659	0
0.66	0.102801353	0.028872998	0.000000093	0.00567259	0.002970996	0.000237785	0
0.67	0.102726353	0.029294824	0.000000994	0.005637026	0.002896691	0.000133628	0
0.68	0.102650076	0.02953573	0.000001752	0.005614671	0.002863283	0.000131087	0
0.69	0.1025721	0.029808951	0.000001443	0.005562974	0.002823337	0.000128787	0
0.7	0.102490671	0.030146947	0.000000311	0.005511062	0.002786163	0.000121991	0

Jg	D3	D4	D5	D6	D7	D8	Extrapolation
0.71	0.10241109	0.030344468	0.000019598	0.005476827	0.002752768	0.000100977	0
0.72	0.102322511	0.030777479	0.000016372	0.005444681	0.002709899	0.000103002	0
0.73	0.102242974	0.030925155	0.000009928	0.005429445	0.002675621	0.000101941	0
0.74	0.102153669	0.031228893	0.00000002	0.005362443	0.002643268	0.000085521	0
0.75	0.102066879	0.03162033	0.00000222	0.005345708	0.002602911	0.000082289	0
0.76	0.101975958	0.031949745	0.000000018	0.005277245	0.002549336	0.000078604	0
0.77	0.10189032	0.032346008	0.000000012	0.005318991	0.002530231	0.000072383	0
0.78	0.101796041	0.032502268	0.00000232	0.005206597	0.002493455	0.000067812	0
0.79	0.101702418	0.032979923	0.000000973	0.005142111	0.002429899	0.00005718	0
0.8	0.10160684	0.033287293	0.00000364	0.005129909	0.002400276	0.000054089	0
0.81	0.101509912	0.034033742	0.000000967	0.005094954	0.002380442	0.000041398	0
0.82	0.101410249	0.034294146	0.000036743	0.005119858	0.002326452	0.000029718	0
0.83	0.101309184	0.034889541	0.000000319	0.00506359	0.002302765	0.000025849	0
0.84	0.101202347	0.035389672	0.000000381	0.004999494	0.002252697	0.000016719	0
0.85	0.101095993	0.035927705	0.000000694	0.004948124	0.00224047	0.000001208	0
0.86	0.100992597	0.036343956	0.000000221	0.00489486	0.002214842	0.000013776	0
0.87	0.100882046	0.036826033	0.000000009	0.00486068	0.002169903	0.000014145	0
0.88	0.100764645	0.037254497	0.000000048	0.004858113	0.002141978	0.000002759	0
0.89	0.100643879	0.037851953	0.000000302	0.004826188	0.002103832	0.000009513	0
0.9	0.100529846	0.03862663	0.000000001	0.00477681	0.002074168	0.000010145	0
0.91	0.100403156	0.03922503	0.000000121	0.00473365	0.002038432	0.000002179	0
0.92	0.100280662	0.039878171	0.000000007	0.00480217	0.002022242	0.000007144	0
0.93	0.10014446	0.040528861	0	0.004681727	0.001988908	0.000000361	0
0.94	0.100010643	0.041248252	0.000000641	0.00463309	0.001945673	0.000022042	0
0.95	0.0998665	0.041928422	0.000000002	0.004627736	0.001924704	0.000007641	0
0.96	0.099720875	0.042671708	0.000000024	0.004588411	0.001891847	0.00000024	0
0.97	0.0995791	0.043480377	0.000000039	0.004637308	0.001862064	0.000000286	0
0.98	0.099429452	0.044320415	0.000000739	0.004544061	0.001845467	0.000000385	0
0.99	0.099269516	0.045139567	0.000000825	0.004502813	0.001808558	0.000000088	0
1	0.099106493	0.046083784	0.000000028	0.004580837	0.001788373	0.000000294	0
1.01	0.098941778	0.046921177	0.000000023	0.004549583	0.001756775	0.000068298	0
1.02	0.098767368	0.047898874	0.000000234	0.004452831	0.001727192	0.000042861	0
1.03	0.098585853	0.048897072	0.000000015	0.004441367	0.001698652	0.000032851	0
1.04	0.09840434	0.049830986	0.000000168	0.004425209	0.001665118	0.000003279	0
1.05	0.098207691	0.050922875	0.000000285	0.004394218	0.001645146	0.000001078	0
1.06	0.098011792	0.051810849	0.000000094	0.004419758	0.001619556	0.000000156	0
1.07	0.097803339	0.052980318	0.000000065	0.004386115	0.001592401	0.000000454	0
1.08	0.097595759	0.053972306	0.000000422	0.004412558	0.001576253	0.000000017	0
1.09	0.097368662	0.055047386	0.000000771	0.004436643	0.001547705	0.000000024	0
1.1	0.097137075	0.056088439	0.000000129	0.004440711	0.001526062	0.000000013	0
1.11	0.096893089	0.057120912	0.000000025	0.004405787	0.001502041	0.000000071	0
1.12	0.096639006	0.058284917	0.000000807	0.00442735	0.001477014	0.000000013	0
1.13	0.096383938	0.059350214	0.000000164	0.004404107	0.001451713	0.000001924	0
1.14	0.096107306	0.060355587	0.000000476	0.00444258	0.001437044	0.000000047	0
1.15	0.095818335	0.061440945	0.000000308	0.00444146	0.001412465	0.000000281	0
1.16	0.095526014	0.062430008	0.00000007	0.004505421	0.001388773	0.000000615	0
1.17	0.09520395	0.063422648	0.000001708	0.004576981	0.001368236	0.000000949	0
1.18	0.094873668	0.064353732	0.000000379	0.004582713	0.001342649	0.000000026	0
1.19	0.094533663	0.065290236	0.000000956	0.004646963	0.001328421	0.000000011	0
1.2	0.09417291	0.066134913	0.000001166	0.004759632	0.001304338	0.000000298	0
1.21	0.093798068	0.066932869	0.000001546	0.004801301	0.001298673	0.000000268	0
1.22	0.09340388	0.067689252	0.000000019	0.004879206	0.001278571	0.000000008	0
1.23	0.092986162	0.068396855	0.000000214	0.005047853	0.001265521	0.000000005	0
1.24	0.092548379	0.069016067	0.000000807	0.005441577	0.001246357	0.000000009	0
1.25	0.092089572	0.069597437	0.000000854	0.043383874	0.001238783	0.000000001	0
1.26	0.091600809	0.070084438	0.000000129	0.047205904	0.001219279	0.000000002	0
1.27	0.091086757	0.070516848	0.000000249	0.04978682	0.001183327	0.000000004	0
1.28	0.090554011	0.070896899	0.000000064	0.051721267	0.001179847	0.000000004	0
1.29	0.089976379	0.071155448	0.063460438	0.053235436	0.048028131	0.000000005	0
1.3	0.089363318	0.071351167	0.063933111	0.054365889	0.049239753	0.000000006	0
1.31	0.088718446	0.07150061	0.064134591	0.055220287	0.049986683	0.000000006	0
1.32	0.088018971	0.071518098	0.064337624	0.055736141	0.050545486	0.000000008	0
1.33	0.087272761	0.071495548	0.06429025	0.056207179	0.050867929	0.047161418	0.022828564
1.34	0.086454481	0.07136524	0.064151372	0.056382437	0.05107257	0.047429981	0.023541812
1.35	0.085585938	0.07111682	0.06384374	0.056413006	0.051046083	0.047571252	0.02403542
1.36	0.084634591	0.070809993	0.063417576	0.056267939	0.050840447	0.047528907	0.024198496
1.37	0.083574736	0.070333197	0.062805882	0.055996922	0.050501811	0.04730322	0.024226741
1.38	0.082379148	0.069741596	0.062118377	0.055496606	0.050013018	0.046839404	0.023919264
1.39	0.081043951	0.068984794	0.06124183	0.054784139	0.049332659	0.046121484	0.023311479
1.4	0.079487863	0.068028999	0.060135231	0.053876951	0.048437795	0.045192649	0.022486914
1.41	0.000000111	0.066817018	0.058758234	0.052679796	0.047343874	0.043972	0.021402272
1.42	0.000000393	0.065212317	0.057050063	0.051061147	0.045816639	0.04230616	0.017646214
1.43	0.000000302	0.000000017	0.054739733	0.048763903	0.04372571	0.039552924	0.014703223
1.44	0.000001328	0.000000019	0.000000207	0.044992833	0.040216496	0.03555027	0.007632733
1.45	0.000002186	0.000000003	0.000000017	0.000002975	0.000000038	0.000000004	0
1.46	0.000000232	0.000000275	0.000000257	0.000003122	0.000000038	0.000000004	0
1.47	0.000001747	0.000000436	0.000000158	0.000003122	0.000000038	0.000000004	0
1.48	0.000000311	0.000000174	0.000000194	0.000003122	0.000000038	0.000000026	0
1.49	0.00000203	0.000000113	0.000000154	0.000003122	0.000000038	0.000000026	0
1.5	0.000001923	0.000000063	0.000000164	0.000003122	0.000000038	0.000000009	0